Steel and Composite Structures, *Vol. 37, No. 1* (*2020*) *51-73*
DOI: https://doi.org/10.12989/scs.2020.37.1.051

Simultaneous resonances of SSMFG cylindrical shells resting on viscoelastic foundations

Kamran Foroutan[a] and Habib Ahmadi*

Faculty of Mechanical and Mechatronics Engineering, Shahrood University of Technology, Shahrood, Iran

(*Received January 15, 2020, Revised September 5, 2020, Accepted September 22, 2020*)

Abstract. The present paper investigates the simultaneous resonance behavior of spiral stiffened multilayer functionally graded (SSMFG) cylindrical shells with internal and external functionally graded stiffeners under the two-term large amplitude excitations. The structure is embedded within a generalized nonlinear viscoelastic foundation which is composed of a two-parameter Winkler-Pasternak foundation augmented by a Kelvin-Voigt viscoelastic model with a nonlinear cubic stiffness. The cylindrical shell has three layers consist of ceramic, FGM, and metal. The exterior layer of the cylindrical shell is rich ceramic while the interior layer is rich metal and the functionally graded material layer is located between these layers. With regard to classical shells theory, von-Kármán equation, and Hook law, the relations of stress-strain are derived for shell and stiffeners. The spiral stiffeners of the cylindrical shell are modeled according to the smeared stiffener technique. According to the Galerkin method, the discretized motion equation is obtained. The simultaneous resonance is obtained using the multiple scales method. Finally, the influences of different material and geometrical parameters on the system resonances are investigated comprehensively.

Keywords: nonlinear vibrations; simultaneous resonance; spiral stiffened FG cylindrical shell; multiple scales method; nonlinear viscoelastic foundation; two-term excitation

1. Introduction

Recently, the stiffened structures made of FG materials are extensively utilized in a wide range of engineering applications. Some researches have focused on the nonlinear resonant behavior of the homogeneous structures, the internal resonances for an axially moving cylinder were reported by Wang *et al.* (2013). The primary resonance behavior of axially moving beams with multiple concentrated masses was presented by Sarigul and Boyaci (2010). Nonlinear vibration for fractionally damped and internal resonant of cylindrical shells under transverse excitations, respectively, was investigated by (Mahmoudkhani *et al.* 2011, Rodrigues *et al.* 2017).

For solving the vibration problem of structures, some researchers have considered different methods. For example, using the multiple-scale method, Wang et al. (2016) investigated the linear and nonlinear free vibrations of an axially moving rectangular plate coupled with a dense fluid having a free surface and Wang and Zu (2017a) presented the instability of longitudinally variable speed viscoelastic plates in contact with ideal liquid, respectively. Utilizing the harmonic balance method, Wang and Yang (2017) studied the porosity-dependent nonlinear forced vibrations of FG piezoelectric plates and Wang and Zu (2017b) the nonlinear vibrations of longitudinally moving FG plates containing porosities and contacting with liquid, respectively. A nonlinear surface-stress-dependent model for vibration analysis of cylindrical nanoscale shells conveying fluid using the Galerkin method was investigated by Wang *et al.* (2018a). The free vibration of a metal foam core sandwich beam embedded in Winkler–Pasternak elastic foundation using the Chebyshev collocation method was studied by Wang and Zhao (2019).

In the field of laminated composite structures, the one-third subharmonic resonance behavior of laminated cylindrical shells under radial harmonic excitations was studied by Li *et al.* (2013). Wang (2014) investigated the large-amplitude vibrations of rotating, laminated composite circular cylindrical shells under radial harmonic excitation in the neighborhood of the lowest resonances. Wang and Liu (2019) presented the free vibration and buckling behavior of polymeric shells reinforced with three-dimensional graphene foams polymer composites. Deflection and vibration analysis of higher-order shear deformable compositionally graded porous plate using the finite element method addressed by Ebrahimi and Habibi (2016). Abe *et al.* (2007) derived the steady-state response by utilizing the shooting method. Javed *et al.* (2016) addressed the free vibration behavior of composite cylindrical shells with non-uniform thickness walls. The resonance behaviors of the laminated circular cylinder were investigated by (Zhang *et al.* 2018, Abe *et al.* 2007). Gao *et al.* (2017) addressed the nonlinear vibration and stability analysis of the composite orthotropic plate rested on the elastic foundation in the thermal environment. Three-dimensional free vibration analysis of cylindrical shells with continuous grading reinforcement was presented by

*Corresponding author, Ph.D.
E-mail: habibahmadif@shahroodut.ac.ir
[a]Ph.D. Student

ISSN: 1229-9367 (Print), 1598-6233 (Online)

Yas and Garmsiri (2010).

Some researchers have studied the vibration behavior analysis of the FG shells. For example, the investigation of resonant response for the FG shallow shells, employing the multiple scales procedure was addressed by Alijani *et al.* (2011). Wang et al. (2019a) studied the nonlinear dynamics of fluid-conveying FG sandwich nanoshells. Gao *et al.* (2018a) investigated the nonlinear dynamic stability of the orthotropic FG cylindrical shell rested on the Winkler-Pasternak elastic foundation under linearly increasing load. The nonlinear vibration analysis of metal foam circular cylindrical shells reinforced with graphene platelets was analyzed by Wang *et al.* (2019b). Khayat *et al.* (2018) presented the free vibration analysis of FG cylindrical shells with different shell theories using the semi-analytical method. Wang *et al.* (2018b) addressed the free thermal vibration of FG cylindrical shells containing porosities. Also, Wang *et al.* (2019c) investigated the thermo-electro-mechanical nonlinear vibration of circular FG piezoelectric cylindrical nanoshells on the Winkler-Pasternak foundation. The nonlinear vibration of FG orthotropic cylinder with nonlinear/linear Winkler-type elastic foundations utilizing the first-order shear deformation theory was studied by (Sofiyev 2016, Sofiyev *et al.* 2017). Wang and Zu (2017c) investigated the nonlinear steady-state responses of longitudinally traveling FG plates immersed in liquid. Also, Wang and Zu (2017d) presented the vibrations of FG rectangular plates with porosities and moving in the thermal environment. Electro-mechanical vibrations of FG piezoelectric plates carrying porosities in the translation state were analyzed by Wang (2018). Sheng and Wang (2018a) reported the vibration of cylindrical shells with FG materials under the parametric and external loading. The resonant analysis of the cylindrical shells with FG material under thermal environments was addressed by Du and Li (2013). Li *et al.* (2018) studied the parametric resonance analysis of cylindrical shells with FG material in thermal environments. Gao *et al.* (2018b) reported the resonance responses of the FG porous cylindrical shell. In this study, the governing equations are derived using Donnell's shell theory in conjunction with von Kármán's kinematic nonlinearity.

A review of the literature mentioned above shows that few studies have been done on the resonant behavior of stiffened cylindrical shells with FG material. Some researches have been performed the resonant analysis of spiral stiffened cylindrical shells with FG material. The primary resonant behavior of stiffened FG cylindrical shells was addressed by Sheng and Wang (2018b), utilizing the multiple scales method. The resonant analysis of FG cylindrical shells with spiral stiffeners was addressed by (Ahmadi 2018, Ahmadi and Foroutan 2019a, b, c). Ahmadi and Foroutan (2019a) presented the Subharmonic and Superharmonic resonance of the system. In this researche, the secondary resonance such as Subharmonic and Superharmonic resonance for the single layer spiral stiffened FG shell under the excitation with one term only considered. Primary resonance for the system with the internal and external stiffeners was considered by (Ahmadi 2018, Ahmadi and Foroutan 2019b) with and without initial imperfection and nonlinear elastic foundation. In these researches, the primary resonance for the single layer spiral stiffened FG shell under the excitation with one term only considered. Recently, Ahmadi and Foroutan (2019c) investigated the combination resonance behavior of a cylindrical shell with porosity material under two-term excitation. In this research, it has assumed that the material to be porous and the spiral stiffener, and nonlinear viscoelastic foundation have not been considered and combination resonance for the single layer FG porous shell only considered. Foroutan and Ahmadi (2020) analyzed a semi-analytical method for the free vibration behavior of spiral stiffened multilayer functionally graded (SSMFG) cylindrical shells under the thermal environment. In this research, the free vibration for the SSMFG cylindrical shell with three modes only numerically considered and the resonance analysis has not been considered, whereas in the proposed work the forced vibration and simultaneous resonances analysis is investigated.

Previous works indicate that there is no study on the simultaneous resonance analysis of the spiral stiffened multilayer functionally graded (SSMFG) cylindrical shells resting on nonlinear viscoelastic foundations with two-term large amplitude excitations. Therefore, the novelties of this work are as: (a) Simultaneous resonances formulation are analytically derived via the method of multiple scales for SSMFG cylindrical shells, (b) Incorporation of the effect of the surrounding nonlinear viscoelastic foundations on the SSMFG cylindrical shells behavior, (c) The cylindrical shell has three layers including the ceramic, FGM and metal, (d) The stiffeners are considered to be functionally graded, (e) Investigation of the effect of the internal and external stiffeners on the SSMFG cylindrical shells behavior. For this, to the model of the system, the smeared stiffeners techniques and classical shell theory in conjunction with the relations of von Kármán's large deformation strain-displacement are used to obtain the nonlinear equations of the system. Then, Galerkin's method is used to discretize the domain. For the investigation of the resonance behaviors of the system, the influences of different material and geometrical parameters on the system are studied.

2. Description of the SSMFG cylindrical shell with the nonlinear viscoelastic foundation

Configuration of the SSMFG cylindrical shell resting on a nonlinear viscoelastic foundation is illustrated in Fig. 1. The considered viscoelastic foundation consists of Pasternak (k_s), Winkler (k_w), and nonlinear cubic (k_{nl}) stiffnesses and a viscous damping element. This type of foundation may cover many aspects of realistic foundations. Thickness, radius, and length of the cylindrical shell are denoted by *h, R,* and *L,* respectively. Also, the width, angles, thickness, and spacing of the stiffeners are indicated by *d*, (θ, β), h_s, and *s,* respectively.

In the present study, it is assumed the SSMFG cylindrical shell has three layers which is demonstrated in Fig. 2. Regarding this figure, the exterior layer of the cylindrical shell is rich ceramic while the interior layer is

rich metal and the functionally graded material layer is located between these layers.

The mass density and Young's modulus of the FG shell and stiffeners are defined as (Nam *et al.* 2018, Foroutan and Ahmadi 2020)

$$[E_{sh}(z), \rho_{sh}(z,)] = \begin{cases} (E_c, \rho_c) \quad ; & -\frac{h}{2} \le z \le -\frac{h}{2} + h_u \\ (E_c, \rho_c) + (E_{mc}, \rho_{mc}) \left(\frac{2z + h - 2h_u}{2h_m}\right)^{K_{sh}} ; & -\frac{h}{2} + h_u \le z \le \frac{h}{2} - h_b \\ (E_m, \rho_m); & \frac{h}{2} - h_b \le z \le \frac{h}{2} \end{cases} \quad (1a)$$

Internal stiffeners

$$\begin{Bmatrix} E_{st}(z) \\ \rho_{st}(z) \end{Bmatrix} = \begin{Bmatrix} E_m \\ \rho_m \end{Bmatrix} + \begin{Bmatrix} E_{cm} \\ \rho_{cm} \end{Bmatrix} \left(\frac{2z - h}{2h_s}\right)^{K_{st}} \quad ; \frac{h}{2} \le z \le \frac{h}{2} + h_s \quad (1b)$$

External stiffeners

$$\begin{Bmatrix} E_{st}(z) \\ \rho_{st}(z) \end{Bmatrix} = \begin{Bmatrix} E_c \\ \rho_c \end{Bmatrix} + \begin{Bmatrix} E_{mc} \\ \rho_{mc} \end{Bmatrix} \left(\frac{2z + h}{2h_s}\right)^{K_{st}} \quad ; -\left(\frac{h}{2} + h_s\right) \le z \le -\frac{h}{2} \quad (1c)$$

where e.g.

$$E_{mc} = E_m - E_c \quad (2)$$

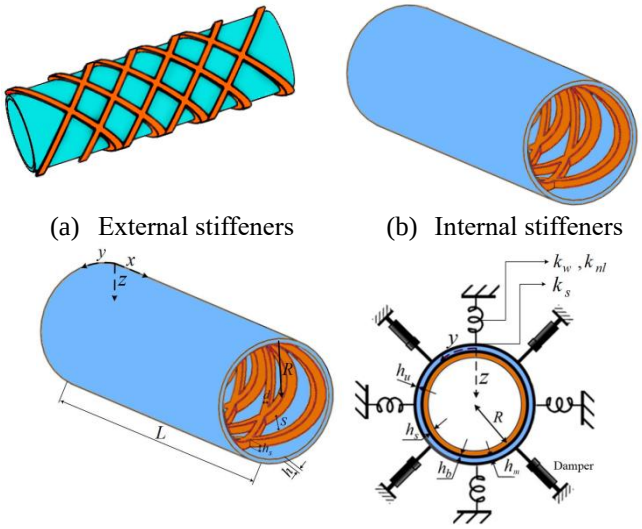

(a) External stiffeners (b) Internal stiffeners

Fig. 1 Schematic of the multilayer FG cylindrical shell with the functionally graded spiral stiffeners and a nonlinear viscoelastic Kelvin-Voigt foundation

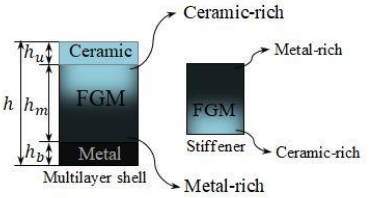

Fig. 2 The material distribution of multilayer cylindrical shell and stiffeners

$K_{st} \ge 0$ and $K_{sh} \ge 0$ are the stiffeners and shell material power-law index, respectively. $\rho_{sh}(z)$, $\rho_{st}(z)$ and $E_{sh}(z)$, $E_{st}(z)$ are mass densities and Young's modulus of the FG stiffeners and shell, respectively. The subscripts st, sh, m, and c refer to the stiffeners, shell, metal, and ceramic, respectively. P is a nonlinear function of temperature which is defined as (Du and Li 2013)

$$\mathrm{P} = P_0(P_{-1}T^{-1} + 1 + P_1T + P_2T^2 + P_3T^3) \quad (3)$$

3. The theoretical formulation

In the light of von Kármán kinematic nonlinearity, the strain-displacement relation becomes (Wang *et al.* 2019d, Zarouni *et al.* 2014)

$$\begin{Bmatrix} \varepsilon_x \\ \varepsilon_y \\ \gamma_{xy} \end{Bmatrix} = \begin{Bmatrix} \varepsilon_x^0 \\ \varepsilon_y^0 \\ \gamma_{xy}^0 \end{Bmatrix} - z \begin{Bmatrix} \kappa_x \\ \kappa_y \\ 2\kappa_{xy} \end{Bmatrix} \quad (4)$$

$$\kappa_x = w_{,xx}, \quad \kappa_y = w_{,yy}, \quad \kappa_{xy} = w_{,xy}$$

where $\kappa_x, \kappa_y, \kappa_{xy}$ are the shell curvature changes and twist. γ_{xy}^0 is the shear strain, and ε_y^0, ε_x^0 are the normal strains. Moreover, the components of the strain on the middle surface of shells are given by (Dat *et al.* 2019, Nam *et al.* 2018, Lezgy-Nazargah *et al.* 2011)

$$\begin{aligned} \varepsilon_x^0 &= u_{,x} + \frac{1}{2}w_{,x}^2 \\ \varepsilon_y^0 &= v_{,y} - \frac{w}{R} + \frac{1}{2}w_{,y}^2 \\ \gamma_{xy}^0 &= u_{,y} + v_{,x} + w_{,x}w_{,y} \end{aligned} \quad (5)$$

where $w = w(x,y)$, $u = u(x,y)$ and $v = v(x,y)$ are the displacement components along z, x, and y axes, respectively.

The compatibility equation according to Eq. (5) can be written as

$$\varepsilon_{x,yy}^0 + \varepsilon_{y,xx}^0 - \gamma_{xy,xy}^0 = -\frac{w_{,xx}}{R} + w_{,xy}^2 - w_{,xx}w_{,yy} \quad (6)$$

The stress-strain relations with regard to the Hooke's law for the cylindrical shell with FG material are

$$\begin{Bmatrix}\sigma_x^{sh}\\ \sigma_y^{sh}\\ \tau_{xy}^{sh}\end{Bmatrix}=\begin{bmatrix}\frac{E_{sh}(z)}{1-\nu^2} & \frac{\nu E_{sh}(z)}{1-\nu^2} & 0\\ \frac{\nu E_{sh}(z)}{1-\nu^2} & \frac{E_{sh}(z)}{1-\nu^2} & 0\\ 0 & 0 & \frac{E_{sh}(z)}{2(1+\nu)}\end{bmatrix}\begin{Bmatrix}\varepsilon_x\\ \varepsilon_y\\ \gamma_{xy}\end{Bmatrix} \tag{7}$$

On the other hand, the constitutive law of the spiral stiffeners is (Foroutan *et al.* 2018, Shaterzadeh and Foroutan 2016)

$$\begin{Bmatrix}\sigma_x^{st}\\ \sigma_y^{st}\\ \tau_{xy}^{st}\end{Bmatrix}=\begin{bmatrix}H_{11} & H_{12} & H_{13}\\ H_{21} & H_{22} & H_{23}\\ H_{31} & H_{32} & H_{33}\end{bmatrix}\begin{Bmatrix}h_1\varepsilon_x\\ h_2\varepsilon_y\\ h_3\gamma_{xy}\end{Bmatrix} \tag{8}$$

where ν is Poisson's ratio. $\sigma_x^{sh},\sigma_y^{sh}$ are the in-plane normal stresses and τ_{xy}^{sh} is the in-plane shearing stress of the cylindrical shell. H_{ij} $(i,j=1,2,3)$ and h_i $(i=1,2,3)$ are presented in appendix A. τ_{xy}^{st} is the in-plane shear stress and $\sigma_x^{st},\sigma_y^{st}$ are the in-plane normal stresses of the spiral stiffener. Utilizing the smeared stiffeners technique, the influence of the stiffeners on the cylindrical shell may be considered. To obtain the resultant moments (M_x,M_y,M_{xy}) and forces (N_x,N_y,N_{xy}) for the spiral stiffened multilayer cylindrical shell with FG material, the equations of stress-strain (7) and (8) are integrated along the thickness direction.

Neglecting the in-plane inertias, the equilibrium equations of cylindrical shells with regard to the classical shell theory are as (Bich *et al.* 2013, Van Dung and Hoa 2013, Dai *et al.* 2013)

$$\begin{aligned}&N_{x,x}+N_{xy,y}=0\\ &N_{xy,x}+N_{y,y}=0\\ &M_{x,xx}+2M_{xy,xy}+M_{y,yy}+N_xw_{,xx}+2N_{xy}w_{,xy}\\ &\quad+N_y\left(w_{,yy}+1/R\ \right)-k_ww+k_s\left(w_{,xx}+w_{,yy}\right)\\ &\quad+k_{nl}w^3+F(t)=\rho_1w_{,tt}+2\rho_1\hat{c}w_{,t}\end{aligned} \tag{9}$$

where $\hat{c}$ is the coefficient of the viscous damping. The harmonic excitation $F(t)$ and the mass density ρ_1 are as follows

Internal stiffeners

$$\rho_1=\left(\rho_c+\frac{\rho_{mc}}{K_{sh}+1}\right)h_m+2\left(\rho_m+\frac{\rho_{cm}}{K_{st}+1}\right)\frac{dh_s}{s}+\rho_ch_u++\rho_mh_b \tag{10a}$$

External stiffeners

$$\rho_1=\left(\rho_m+\frac{\rho_{cm}}{K_{sh}+1}\right)h_m+2\left(\rho_c+\frac{\rho_{mc}}{K_{st}+1}\right)\frac{dh_s}{s}+\rho_ch_u++\rho_mh_b \tag{10b}$$

Harmonic excitation

$$F(t)=Q_1\cos(\Omega_1t+\theta_1)+Q_2\cos(\Omega_2t+\theta_2) \tag{10c}$$

where Q_1 and Q_2 are the load amplitudes. In the real engineering application, the applied excitation on the system is including several frequencies. So, in this study, we have assumed that the excitation consists of two frequencies (see Eq. (10c)), and then according to the double-frequency excitation, we have tried to analyze the simultaneous resonances of the system. The first two equations of Eq. (9) may be satisfied merely by definition of the following stress function (ψ)

$$N_x=\psi_{,yy};\quad N_y=\psi_{,xx};\quad N_{xy}=-\psi_{,xy} \tag{11}$$

To find the compatibility equation with regard to the lateral deflection w and the stress function ψ, first, the strain components must be obtained in terms of the resultant forces. So, according to Eq. (11), the strain components may be expressed in terms of the stress function. Substituting these relations into the compatibility Eq. (6), and omitting the displacement components of in-plane partial differentials, the compatibility equation may be represented in terms of w and ψ (Foroutan *et al.* 2018, Shaterzadeh and Foroutan 2016)

$$\begin{aligned}&J_{11}^*\psi_{,xxxx}+(J_{33}^*-J_{12}^*+J_{21}^*)\psi_{,xxyy}+J_{22}^*\psi_{,yyyy}\\ &\quad+J_{21}^{**}w_{,xxxx}+(J_{11}^{**}+J_{22}^{**}-2J_{36}^{**})w_{,xxyy}\\ &\quad+J_{12}^{**}w_{,yyyy}+\frac{1}{R}w_{,xx}+\left[w_{,xy}^2-w_{,xx}w_{,yy}\right]=0\end{aligned} \tag{12}$$

where J_{ij}^*,J_{ij}^{**} are presented in Appendix B.

Similar to the above discussion, by substituting the moment resultants into the third part of Eq. (9) and utilizing Eqs. (5) and (10) yields (Foroutan *et al.* 2018, Pendhari *et al.* 2012)

$$\begin{aligned}&\rho_1w_{,tt}+2\rho_1\hat{c}w_{,t}+A_{11}^{**}w_{,xxxx}+A_{22}^{**}w_{,yyyy}\\ &\quad+(A_{12}^{**}+A_{21}^{**}+4A_{36}^{**})w_{,xxyy}-A_{21}^*\psi_{,xxxx}\\ &\quad-(A_{11}^*+A_{22}^*-2A_{36}^*)\psi_{,xxyy}-A_{12}^*\psi_{,yyyy}\\ &\quad-\frac{1}{R}\psi_{,xx}-\psi_{,yy}w_{,xx}+2\psi_{,xy}w_{,xy}-\psi_{,xx}w_{,yy}\\ &\quad-Q_1\cos(\Omega_1t+\theta_1)-Q_2\cos(\Omega_2t+\theta_2)\\ &\quad+k_ww-k_s\left(w_{,xx}+w_{,yy}\right)-k_{nl}w^3=0\end{aligned} \tag{13}$$

where the coefficients A_{ij}^* and A_{ij}^{**} are presented in Appendix B.

4. The semi-analytical solutions of the problem

4.1 Single mode analysis

When the system does not possess an internal resonance the modes are uncoupled, and we can consider the superharmonic and subharmonic resonances for the each of mode independently. So, in this research, it is assumed that the internal resonance is not occurred. Therefore, the forms of the approximate solution of the simply supported SSFG cylindrical shells are considered as follows (Dai *et al.* 2013, Wang *et al*. 2019d, Pendhari *et al.* 2012, Foroutan *et al.* 2019) to solve Eq. (12)

$$w(x,y,t)=W_{mn}(t)\sin\frac{m\pi x}{L}\sin\frac{ny}{R} \tag{14}$$

where n and m are numbers of the half and full waves of

deformation in the circumferential and axial directions, respectively. $W_{mn}(t)$ represents the deflection amplitude.

Substituting Eq. (14) in Eq. (12), and then solving the resultant equation for ψ, yields

$$\psi = \psi_1 \cos\frac{2m\pi x}{L} + \psi_2 \cos\frac{2ny}{R} - \psi_3 \sin\frac{m\pi x}{L}\sin\frac{ny}{R} \tag{15}$$

The $\psi_i (i = 1,2,3)$ are as follows

$$\psi_1 = \frac{n^2\lambda^2}{32J_{11}^* m^2\pi^2} W_{mn}(t)(W_{mn}(t)+\mu h)(W_{mn}(t)+2\mu h)$$

$$\psi_2 = \frac{m^2\pi^2}{32J_{22}^* n^2\lambda^2} W_{mn}(t)(W_{mn}(t)+\mu h)(W_{mn}(t)+2\mu h) \tag{16}$$

$$\psi_3 = \frac{B}{A} W_{mn}(t)$$

If Eq. (13) is denoted by $\mathbb{G}= 0$, the relevant W_{mn} terms may be found based on Galerkin's method as

$$\int_0^L \int_0^{2\pi R} \sin\frac{m\pi x}{L}\sin\frac{ny}{R}\Gamma dydx \tag{17}$$

After substituting Eqs. (14) and (15) into Eq. (13), the following results may be obtained, after carrying out Galerkin's orthogonally integration appeared in Eq. (17)

$$\ddot{W}_{mn} + 2\hat{c}\dot{W}_{mn} + \omega_{mn}^2 W_{mn} + \hat{a}_3 W_{mn}^3 = k_1\cos(\Omega_1 t + \theta_1) + k_2\cos(\Omega_2 t + \theta_2) \tag{18}$$

where

$$\omega_{mn} = \left[\frac{1}{L^4\rho_1}\left(D + \frac{BB^*}{A} + L^4 k_w + L^2 k_s[(\lambda n)^2 + (m\pi)^2]\right)\right]^{\frac{1}{2}} \tag{19}$$

$$k_1 = \frac{Q_1}{L^4\rho_1}, \quad k_2 = \frac{Q_2}{L^4\rho_1}$$

where B, A, D, and B^* are presented in Appendix B. ω_{mn} is the dominant natural frequency of the cylindrical shell, and $\hat{a}_3$ expressions that are case-dependent and defined in the sequel.

4.2 Multi modes analysis

Here, in order to derive the discretized equation of motion for different modes, the four prominent order modes are considered in the following form (for $m = 1$ and $n = 1,3$). These relationships are extracted to investigate the system assuming internal resonance. It should be noted that the simultaneous resonance by considering the internal resonance 1:1:3:3, for this system is investigated.

$$w(x,y,t) = W_1(t)\sin\frac{\pi x}{L}\sin\frac{y}{R} + W_2(t)\sin\frac{\pi x}{L}\cos\frac{y}{R} + W_3(t)\sin\frac{\pi x}{L}\sin\frac{3y}{R} + W_4(t)\sin\frac{\pi x}{L}\cos\frac{3y}{R} \tag{20}$$

Substituting Eq. (20) in Eq. (12), and then solving the resultant equation for ψ_a, yields

$$\begin{aligned}\psi_a = {} & \psi_1\cos\frac{2y}{R} + \psi_2\cos\frac{4y}{R} + \psi_3\cos\frac{2y}{R} + \psi_4\cos\frac{4y}{R} \\ & + \psi_5\cos\left(\frac{2\pi Rx + 6Ly}{LR}\right) + \psi_6\cos\left(\frac{-\pi Rx + Ly}{LR}\right) \\ & + \psi_7\cos\left(\frac{2\pi Rx + 2Ly}{LR}\right) + \psi_8\cos\left(\frac{\pi Rx + 3Ly}{LR}\right) \\ & + \psi_9\cos\left(\frac{-\pi Rx + 3Ly}{LR}\right) + \psi_{10}\cos\left(\frac{\pi Rx + Ly}{LR}\right) \\ & + \psi_{11}\sin\left(\frac{2\pi Rx + 6Ly}{LR}\right) + \psi_{12}\sin\left(\frac{\pi Rx + Ly}{LR}\right) \\ & + \psi_{13}\sin\left(\frac{2\pi Rx + 2Ly}{LR}\right) + \psi_{14}\sin\left(\frac{\pi Rx + 3Ly}{LR}\right) \\ & + \psi_{15}\sin\left(\frac{-\pi Rx + Ly}{LR}\right) + \psi_{16}\sin\left(\frac{2\pi Rx + 4Ly}{LR}\right) \\ & + \psi_{17}\sin\left(\frac{-\pi Rx + 3Ly}{LR}\right) \\ & + \psi_{18}\cos\left(\frac{2\pi Rx + 4Ly}{LR}\right) \\ & + \psi_{19}\cos\left(\frac{-2\pi Rx + 4Ly}{LR}\right) \\ & + \psi_{20}\cos\left(\frac{-2\pi Rx + 2Ly}{LR}\right) \\ & + \psi_{21}\cos\left(\frac{-2\pi Rx + 6Ly}{LR}\right) \\ & + \psi_{22}\sin\left(\frac{-2\pi Rx + 4Ly}{LR}\right) \\ & + \psi_{23}\sin\left(\frac{-2\pi Rx + 2Ly}{LR}\right) \\ & + \psi_{24}\sin\left(\frac{-2\pi Rx + 6Ly}{LR}\right) + \psi_{25}x^4\end{aligned} \tag{21}$$

where the coefficients ψ_i $(i = 1,2,\ldots,25)$ are function of π, R, L, J_{ij}^*, J_{ij}^{**}, $W_1(t)$, $W_2(t)$, $W_3(t)$, and $W_4(t)$. Although they are too long to be explicitly written here, they can be easily computed with computer algebra. If equation of motion (Eq. (13)) is denoted by $\mathbb{G}= 0$, we can write Galerkin's method as

$$\begin{aligned}&\int_0^L\int_0^{2\pi R}\sin\frac{\pi x}{L}\sin\frac{y}{R}\Gamma dydx \\ &\int_0^L\int_0^{2\pi R}\sin\frac{\pi x}{L}\cos\frac{y}{R}\Gamma dydx \\ &\int_0^L\int_0^{2\pi R}\sin\frac{\pi x}{L}\sin\frac{3y}{R}\Gamma dydx \\ &\int_0^L\int_0^{2\pi R}\sin\frac{\pi x}{L}\cos\frac{3y}{R}\Gamma dydx\end{aligned} \tag{22}$$

After substituting Eqs. (20) and (21) into Eq. (13), substituting the outcome into Eq. (22), and after carrying out Galerkin's orthogonally integration appeared in Eq. (22), the following results can be obtained

$$\begin{aligned}
&\ddot{W}_1 + 2\hat{c}\dot{W}_1 + \omega_1^2 W_1 + g_{11}W_1^3 + g_{12}W_3W_1^2 \\
&\quad + g_{13}W_1W_2^2 + g_{14}W_3W_2^2 + g_{15}W_1W_3^2 \\
&\quad + g_{16}W_1W_4^2 + g_{17}W_1W_2W_4 = g_{18}F(t) \\
&\ddot{W}_2 + 2\hat{c}\dot{W}_2 + \omega_2^2 W_2 + g_{21}W_2^3 + g_{22}W_2W_1^2 \\
&\quad + g_{23}W_4W_1^2 + g_{24}W_4W_2^2 + g_{25}W_2W_3^2 \\
&\quad + g_{26}W_2W_4^2 + g_{27}W_1W_2W_3 = g_{28}F(t) \\
&\ddot{W}_3 + 2\hat{c}\dot{W}_3 + \omega_3^2 W_3 + g_{31}W_1^3 + g_{32}W_3W_1^2 \\
&\quad + g_{33}W_1W_2^2 + g_{34}W_3W_2^2 + g_{35}W_3^3 \\
&\quad + g_{36}W_3W_4^2 = g_{37}F(t) \\
&\ddot{W}_4 + 2\hat{c}\dot{W}_4 + \omega_4^2 W_4 + g_{41}W_2^3 + g_{42}W_2W_1^2 \\
&\quad + g_{43}W_4W_1^2 + g_{44}W_4W_2^2 + g_{45}W_4W_3^2 \\
&\quad + g_{46}W_4^3 = g_{28}F(t)
\end{aligned} \tag{23}$$

where the coefficients g_{ij}, and ω_i are function of π, R, L, J_{ij}^{*}, J_{ij}^{**}, A_{ij}^{*}, A_{ij}^{**}, k_w, k_s, and k_{nl}. Although they are too long to be explicitly written here, they can be easily computed with computer algebra.

5. The semi-analytical solutions of the problem

5.1 Single mode solution

According to Eq. (18), the nonlinearity and the damping terms must be assumed in the same order. Accordingly, the damping and cubic nonlinearity (W_{mn}^3) terms of Eq. (18) must be set in the same order (Nayfeh and Mook 1995). In this case, $\hat{a}_3$ parameters become

$$\hat{c} = \epsilon c, \qquad \hat{a}_3 = \epsilon \alpha_3 \tag{24}$$

where

$$\alpha_3 = \frac{G}{L^4\rho_1} + \frac{9}{16\rho_1}k_{nl} \tag{25}$$

Also, dimensionless parameter $\epsilon \ll 1$ is the order of the motion amplitude, and G is defined in Appendix B.

Substituting Eq. (24) in Eq. (18), the nonlinear equation of the system becomes as follows

$$\begin{aligned}
&\ddot{W}_{mn} + 2\epsilon c\dot{W}_{mn} + \omega_{mn}^2 W_{mn} + \epsilon\alpha_3 W_{mn}^3 = \\
&\qquad k_1\cos(\Omega_1 t + \theta_1) + k_2\cos(\Omega_2 t + \theta_2)
\end{aligned} \tag{26}$$

5.1.1 Solution of the resulting nonlinear equation by the multiple scales method

For solving Eq. (26) utilizing the multiple scales method, an expansion in the following form is adopted

$$\mathrm{W}(t,\epsilon) = W_0(T_0,T_1) + \epsilon W_1(T_0,T_1) + \cdots \tag{27}$$

where the new time-dependent variables T_0 and T_1 are introduced as

$$T_n = \epsilon^n t; \qquad n = 0,1 \tag{28}$$

Substitution of Eq. (27) in Eq. (26), and then equating the coefficients of the ϵ^0 and ϵ (perturbation coefficients) to zero leads to

$$\begin{aligned}
&D_0^2 W_0 + \omega_{mn}^2 W_0 = k_1\cos(\Omega_1 t + \theta_1) \\
&\qquad + k_2\cos(\Omega_2 t + \theta_2)
\end{aligned} \tag{29}$$

$$\begin{aligned}
&D_0^2 W_1 + \omega_{mn}^2 W_1 = \\
&\qquad -2D_0D_1W_0 - 2cD_0W_0 - \alpha_3 W_0^3
\end{aligned} \tag{30}$$

where

$$D_n = \frac{\partial}{\partial T_n}; \qquad n = 0,1 \tag{31}$$

The general solution of Eq. (29) is

$$W_0 = A(\ T_1)e^{i\omega_{mn}T_0} + \Lambda_1 e^{i\Omega_1 T_0} + \Lambda_2 e^{i\Omega_2 T_0} + \mathrm{c.c.} \tag{32}$$

In Eq. (32), $\mathrm{c.c.}$ is the complex conjugate and

$$\Lambda_1 = \frac{k_1 e^{i\theta_1}}{2(\omega_{mn}^2 - \Omega_1^2)}, \qquad \Lambda_2 = \frac{k_2 e^{i\theta_2}}{2(\omega_{mn}^2 - \Omega_2^2)} \tag{33}$$

Substituting Eq. (32) in Eq. (30), yields

$$\begin{aligned}
&D_0^2 W_1 + \omega_{mn}^2 W_1 = -[2i\omega_{mn}(A' + cA) \\
&+3\alpha_3(A\Lambda + 2\Lambda_1\bar{\Lambda}_1 + 2\Lambda_2\bar{\Lambda}_2)A]e^{i\omega_{mn}T_0} \\
&-\Lambda_1[2i\Omega_1 c + 3\alpha_3(2A\bar{A} + \Lambda_1\bar{\Lambda}_1 + 2\Lambda_2\bar{\Lambda}_2)]e^{i\Omega_1 T_0} \\
&-\Lambda_2[2i\Omega_1 c + 3\alpha_3(2A\bar{A} + 2\Lambda_1\bar{\Lambda}_1 + \Lambda_2\bar{\Lambda}_2)]e^{i\Omega_2 T_0} \\
&-\alpha_3\{A^3 e^{3i\omega_{mn}T_0} + \Lambda_1^3 e^{3i\Omega_1 T_0} + \Lambda_2^3 e^{3i\Omega_2 T_0} \\
&+3A^2\Lambda_1 e^{i(2\omega_{mn}+\Omega_1)T_0} + 3A^2\Lambda_2 e^{i(2\omega_{mn}+\Omega_2)T_0} \\
&+3A^2\bar{\Lambda}_1 e^{i(2\omega_{mn}-\Omega_1)T_0} + 3A^2\bar{\Lambda}_2 e^{i(2\omega_{mn}-\Omega_2)T_0} \\
&+3A\Lambda_1^2 e^{i(\omega_{mn}+2\Omega_1)T_0} + 3A\Lambda_2^2 e^{i(\omega_{mn}+2\Omega_2)T_0} \\
&+3A\bar{\Lambda}_1^2 e^{i(\omega_{mn}-2\Omega_1)T_0} + 6A\bar{\Lambda}_1\Lambda_2 e^{i(\omega_{mn}-\Omega_1+\Omega_2)T_0} \\
&+6A\Lambda_1\bar{\Lambda}_2 e^{i(\omega_{mn}+\Omega_1-\Omega_2)T_0} + 3\Lambda_1^2\Lambda_2 e^{i(2\Omega_1+\Omega_2)T_0} \\
&+3\Lambda_1^2\bar{\Lambda}_2 e^{i(2\Omega_1-\Omega_2)T_0} + 3\Lambda_1\Lambda_2^2 e^{i(\Omega_1+2\Omega_2)T_0} \\
&+3\bar{\Lambda}_1\Lambda_2^2 e^{i(2\Omega_2-\Omega_1)T_0}\} + \mathrm{c.c.}
\end{aligned} \tag{34}$$

Eq. (34) shows the several resonant combinations that some of them are mono frequency excitations and others are multi-frequency excitations. These combinations can be considered in the following form

Subharmonic resonance

$$\omega_{mn} \approx \frac{1}{3}\Omega_k \tag{35}$$

Superharmonic resonance

$$\omega_{mn} \approx 3\Omega_k \tag{36}$$

Combination resonance

$$\begin{aligned}
&\omega_{mn} \approx |\pm 2\Omega_l \pm \Omega_k| \\
&\omega_{mn} \approx \frac{1}{2}(\Omega_l \pm \Omega_k)
\end{aligned} \tag{37}$$

where $k, l = 1, 2$. It should be noted that for a multifrequency excitation, several resonant conditions may be occurred simultaneously; i.e., both superharmonic and combination resonances or both subharmonic and superharmonic resonances, etc. can occur simultaneously. For a two-term excitation, maximum two resonances can be occurred simultaneously. If excitation frequencies are depicted by Ω_1 and Ω_2 where $\Omega_2 > \Omega_1$, the possible secondary resonances can be occurred in the following form

$$\begin{gathered}\omega_{mn} \approx 3\Omega_1 \quad \text{or} \quad 3\Omega_2 \\ \omega_{mn} \approx \frac{1}{3}\Omega_1 \quad \text{or} \quad \frac{1}{3}\Omega_2 \\ \omega_{mn} \approx \Omega_2 \pm 2\Omega_1 \quad \text{or} \quad 2\Omega_1 - \Omega_2 \\ \omega_{mn} \approx 2\Omega_2 \pm \Omega_1 \\ \omega_{mn} \approx \frac{1}{2}(\Omega_2 \pm \Omega_1)\end{gathered} \tag{38}$$

Investigation of these resonances shows that more than one of them occurs simultaneously if

(a) $\Omega_2 \approx 9\Omega_1 \approx 3\omega_{mn}$

(b) $\Omega_2 \approx \Omega_1 \approx 3\omega_{mn}$

(c) $\Omega_2 \approx \Omega_1 \approx \frac{1}{3}\omega_{mn}$

(d) $\Omega_2 \approx 5\Omega_1 \approx \frac{5}{3}\omega_{mn}$

(e) $\Omega_2 \approx 7\Omega_1 \approx \frac{7}{3}\omega_{mn}$

(f) $\Omega_2 \approx 2\Omega_1 \approx \frac{2}{3}\omega_{mn}$

(g) $\Omega_2 \approx \frac{7}{3}\Omega_1 \approx 7\omega_{mn}$

(h) $\Omega_2 \approx \frac{5}{3}\Omega_1 \approx 5\omega_{mn}$ (39)

Here, the case (a) i.e. simultaneous resonance is selected. In this section, we consider a case of double resonance in which subharmonic and superharmonic resonances exist simultaneously. For frequency analysis purposes, we introduce the two detuning parameters σ_1 and σ_2 as follows

$$3\Omega_1 = \omega_{mn} + \epsilon\sigma_1 \quad \text{and} \quad \Omega_2 = 3\omega_{mn} + \epsilon\sigma_2 \tag{40}$$

Now, Eq. (40) is substituted into Eq. (34), and then the coefficient of secular terms (i.e. $\exp(i\omega_{mn}T_0)$) is set equal to zero as

$$\begin{aligned}&2i\omega_{mn}(A' + cA) + 3\alpha_3(A\bar{A} + 2\Lambda_1\bar{\Lambda}_1 + 2\Lambda_2\bar{\Lambda}_2)A \\ &\quad +\alpha_3\Lambda_1^3 e^{i\sigma_1 T_1} + 3\alpha_3\bar{A}^2\Lambda_2 e^{i\sigma_2 T_1} = 0\end{aligned} \tag{41}$$

To find the response of Eq. (41), A is assumed in the following polar form

$$A = \frac{1}{2}ae^{i\beta} \tag{42}$$

where $\beta(T_1)$ and $a(T_1)$ are real quantities.

After substituting Eq. (42) into Eq. (41), the imaginary and real parts of the resulted equation are obtained as

$$\begin{aligned}&a' + \mu a - \alpha_3\ \Gamma_1 \sin(\sigma_1 T_1 + 3\theta_1 - \beta) \\ &\quad +\alpha_3\ \Gamma_2 a^2 \sin(\sigma_2 T_1 + \theta_2 - 3\beta) = 0\end{aligned} \tag{43}$$

$$\begin{aligned}&a\beta' + \frac{3\alpha_3}{8\omega_{mn}}a^3 + \alpha_3\ \Gamma_3 a + \\ &\quad +\alpha_3\ \Gamma_1 \cos(\sigma_1 T_1 + 3\theta_1 - \beta) \\ &\quad +\alpha_3\ \Gamma_2 a^2 \cos(\sigma_2 T_1 + \theta_2 - 3\beta) = 0\end{aligned} \tag{44}$$

where

$$\begin{aligned}\Gamma_1 &= \frac{1}{8}k_1^3\omega_{mn}^{-1}(\omega_{mn}^2 - \Omega_1^2)^{-3} \\ \Gamma_2 &= \frac{3}{8}k_2\omega_{mn}^{-1}(\omega_{mn}^2 - \Omega_1^2)^{-1} \\ \Gamma_3 &= \frac{3}{4}\omega_{mn}^{-1}[k_1^2(\omega_{mn}^2 - \Omega_1^2)^{-2} + k_2^2(\omega_{mn}^2 - \Omega_2^2)^{-2}]\end{aligned} \tag{45}$$

Eq. (45) according to Eq. (40) can rewrite as follows

$$\begin{aligned}\Gamma_1 &= \frac{749}{4096}k_1^3\omega_{mn}^{-7} + O(\epsilon) \\ \Gamma_2 &= \frac{3}{64}k_2\omega_{mn}^{-3} + O(\epsilon) \\ \Gamma_3 &= \frac{3}{256}\omega_{mn}^{-5}[81k_1^2 + k_2^2] + O(\epsilon)\end{aligned} \tag{46}$$

Regarding Eq. (43), the steady-state motion (i.e., $a' = 0$) exists if, and only if, both $\sigma_1 T_1 - \beta$ and $\sigma_2 T_1 - 3\beta$ are constants. That is

$$\sigma_1 = \beta' \quad \text{and} \quad \sigma_2 = 3\ \beta' \tag{47}$$

So, the steady-state motion exists only when $\sigma_2 = 3\sigma_1 = 3\sigma$. Therefore, Eqs. (43) and (44) illustrate that they correspond to the solutions of following equations

$$\begin{aligned}&\mu a + \alpha_3\ \Gamma_1 \sin(\gamma + 3\theta_1) + \alpha_3\ \Gamma_2 a^2 \sin(\gamma + \theta_2) \\ &\quad = 0\end{aligned} \tag{48}$$

$$\begin{aligned}&-a\sigma + \frac{3\alpha_3}{8\omega_{mn}}a^3 + \alpha_3\ \Gamma_3 a + \\ &\quad +\alpha_3\ \Gamma_1 \cos(\gamma + 3\theta_1) \\ &\quad + \alpha_3\ \Gamma_2 a^2 \cos(\gamma + \theta_2) = 0\end{aligned} \tag{49}$$

5.2 Multi modes solution

In this sub-section, the case of 1:1:3:3 internal resonance and simultaneous resonance are considered. If the relations of natural frequencies are considered as follow, an internal resonance is occurred, and some new secular terms are created.

$$\begin{gathered}3\Omega_1 = \omega_1 + \epsilon\sigma_1;\ \ \Omega_2 = 3\omega_1 + \epsilon\sigma_2 \\ \omega_2 = \omega_1 + \epsilon\sigma_3;\ \ \omega_3 = 3\omega_1 + \epsilon\sigma_4 \\ \omega_4 = 3\omega_1 + \epsilon\sigma_5\end{gathered} \tag{50}$$

Similar to the previous sub-section and according to Eq. (50), the coefficient of secular terms is set equal to zero (solvability equation). It should be noted that the general solution for the coefficients of the ϵ^0 are as follows

$$W_{i0} = A_i(\ T_1)e^{i\omega_i T_0} + \Lambda_1 e^{i\Omega_1 T_0} + \Lambda_2 e^{i\Omega_2 T_0} + \text{c. c.} \tag{51}$$

$i = 1,2,\dots,4$

Then, to solve the solvability equation, $A_i (i = 1,2,\dots,4)$ is assumed in the following form

$$A_i = x_i + ix_{i+1} \tag{52}$$

In Eq. (52), $x_i(i = 1,2,\dots,8)$ are the functions with respect to the amplitude and phase of nonlinear vibrations of the SSMFG cylindrical shell. After substituting Eq. (52) into the solvability equation, the imaginary and real parts of the resultant equations are obtained. These equations will be solved using a numerical method.

6. Results and discussions

6.1 Verification of the results

Results are first verified by those published already by other researchers for special cases. First, the obtained natural frequencies of isotropic cylindrical shells are validated with those presented by (Pellicano 2007, Qin *et al.* 2017, Wang *et al.* 2019d), which is shown in Table 1. Furthermore, the present results of the natural frequencies are compared in Table 2, for the vibration behavior of a cylindrical shell with FG material which is stiffened by stringer and ring, with those accomplished already by Van Dung and Nam (2014).

For more validation of the approach, the present results of the dimensionless natural frequencies ($\bar{\omega}_{mn} = \omega_{mn}R\sqrt{(1-\nu^2)\frac{\rho}{E}}$) are compared in Table 3 with those of the nonlinear vibration behavior of a homogeneous cylindrical shell rested on a Winkler foundation accomplished already by (Sofiyev *et al.* 2009, Van Dung and Nam 2014).

Table 1 Comparison of the natural frequencies (Hz) of cylindrical shell

m	n	Present	Qin *et al.* (2017)	Pellicano (2007)	Wang *et al.* (2019d)
1	7	486.0	484.6	484.6	484.55
1	8	490.3	489.6	489.6	489.55
1	9	545.8	546.2	546.2	546.20
1	6	555.8	553.3	553.3	553.33
1	10	634.8	636.8	636.8	636.81
1	5	728.5	722.1	722.1	722.13
1	11	746.6	750.7	750.7	750.66
1	12	875.5	882.2	882.2	882.23
2	10	962.3	968.1	968.1	968.09
2	11	976.6	983.4	983.4	983.34

Table 2 Comparison of the natural frequencies (rad/s) of stifnened FG cylindrical shell ($L = 0.75$ m, $R = 0.5$ m, $R/h = 250$, $m = 1$, $E_m = 7 \times 10^{10}\,\mathrm{N/m^2}$, $\rho_m = 2702\,\mathrm{kg/m^3}$, $E_c = 38 \times 10^{10}\,\mathrm{N/m^2}$, $\rho_c = 3800\,\mathrm{kg/m^3}$, $\nu = 0.3$, $d_s = d_r = 0.0025$ m, $h_s = h_r = 0.01$ m)

	Present	Van Dung and Nam (2014)	Errors (%)
Un-stiffened	1654.05	1654.05	0.00
Internal stiffeners	2539.43	2539.43	0.00
External stiffeners	2518.90	2518.90	0.00

Table 3 A comparison of the dimensionless natural frequencies of the cylindrical shell resting on the Winkler foundation ($L/R = 2$, $R/h = 100$, $k_w = 10^4\ \mathrm{N/m^3}$)

(*m*,*n*)	Present	Sofiyev *et al.* (2009)		Van Dung and Nam (2014)	
			Errors (%)		Errors (%)
(1,1)	0.67480	0.67921	0.65	0.67480	0.00
(1,2)	0.36223	0.36463	0.66	0.36223	0.00
(1,3)	0.20670	0.20804	0.65	0.20670	0.00

Table 4 Results of the natural frequencies (Hz) of the stiffened cylindrical shell ($L = 0.6096$ m, $R = 0.242$ m, $h = 0.65 \times 10^{-3}$ m, $E = 68.95 \times 10^9\,\mathrm{N/m^2}$, $\rho = 2714\,\mathrm{kg/m^3}$, $\nu = 0.3$, $n_s = 60$)

(*m*,*n*)	Present	Mustafa and Ali (1989)	Errors (%)
(1,5)	228.1	226	0.9
(1,6)	189.4	191	0.8
(1,7)	174.0	179	2.4

Also, results of a stiffened cylindrical shell are compared with the experimentally validated results of Mustafa and Ali (1989) in Table 4. It may easily be noted that there is a good agreement among these results.

Finally, a numerical method is used to verify the results of the proposed analytical method for simultaneous resonance. Hereafter, the material characteristics of the system are shown in Table 5. Also, the foundation and geometric specifications of the shell and stiffeners are listed in Table 6. The geometric parameters and material parameters listed in Table 5 will be used for the simulation results.

In the numerical procedure, Eq. (18) has been solved via the fourth-order Runge-Kutta procedure. In this method, the maximum amplitude has been detected for various magnitudes of the excitation, based on the time responses, using the $W(0) = 0$ and $\dot{W}(0) = 0$ initial conditions. The analytical and numerical frequency response curves are compared in Fig. 3. This figure shows that the results of the analytical method are almost similar to the results of the numerical method, especially, in the vicinity of the stability.

6.2 Comprehensive parametric studies on the simultaneous resonances

Now, the effects of various factors on the spirally stiffened multilayer FG cylindrical shells surrounded by nonlinear viscoelastic foundations under two-term large amplitude excitations are illustrated. In this regard, the influences of the material and geometric parameters, and nonlinear viscoelastic foundation are considered.

In Fig. 4, a typical frequency-response graph for multilayer FG cylindrical shells without stiffeners is shown. The various solid and dotted branches indicate stable and unstable solutions, respectively Regarding Fig. 4, it is

Table 5 The material, foundation, and geometric specifications of the shell

R(m)	L(m)	h_m(m)	h_u(m)	h_b(m)	h_s(m)	d(mm)	n_s	m	ν	k_w (kN/m^3)	k_s (kN/m)	k_{nl} (MN/m^5)
0.5	0.75	0.0012	0.0004	0.0004	0.01	2.5	40	1	0.3	10^6	10^4	10^{10}

Table 6 Material properties of the considered SSMFG cylindrical shells (Duc and Thang 2015)

Material	Properties	P_0	P_{-1}	P_1	P_2	P_3
Si_3N_4	E(Pa)	3.48e11	0	-3.07e-4	2.16e-7	-8.95e-11
(Ceramic)	ρ(Kg/m^3)	2370	0	0	0	0
	α(K^{-1})	5.87e-6	0	9.10e-4	0	0
	K(W/mK)	13.723	0	0	0	0
SUS304	E(Pa)	2.01e11	0	3.08e-4	-6.53e-7	0
(Metal)	ρ(Kg/m^3)	8166	0	0	0	0
	α(K^{-1})	1.23e-5	0	8.09e-4	0	0
	K(W/mK)	15.379	0	0	0	0

observed that there are five saddle bifurcations with various intermediate stable and unstable branches. Considering Fig. 4, the two branches A and D are related to the superharmonic resonance state, the two branches B and C are for subharmonic resonance state. When we look at Fig. 4, in the increasing direction of detuning parameter, before of the first saddle bifurcation, there are on stable nontrivial branches. At the area between two first saddle bifurcations, there are three nontrivial branches, which one of them is unstable and two others are stable. At the area between two first saddle bifurcations, there are three nontrivial branches, which one of them is unstable and two others are stable. At the area between second and third saddle bifurcations, there are five nontrivial branches, which two of them are unstable and three others are stable. Finally, at the area between third and fourth saddle bifurcations, there are seven nontrivial branches, which three of them are unstable and four others are stable. When there are several branches, the initial condition help to recognize the right solution.

Also, to study the stability of the steady-state response according to Wang *et al.* (2017), we must consider a new variable including the equilibrium point and perturbation parameters related to this point, and then substitute this variable in Eqs. (39) and (40). Then by eliminating the nonlinear term in the outcome equation, we obtain a set of linear equations. Now, if all the eigenvalues of the Jacobian matrix of this equations, the matrix of the coefficients in outcome equations, have a negative real part, the corresponding steady-state responses are stable. If the eigenvalues of the Jacobian matrix have at least one positive real part, the corresponding steady-state responses are instable.

The influence of the stiffener angles on the response of the amplitude-frequency for the internal and external spiral stiffened cylindrical shell with FG material is displayed in Figs. 5 and 6, respectively.

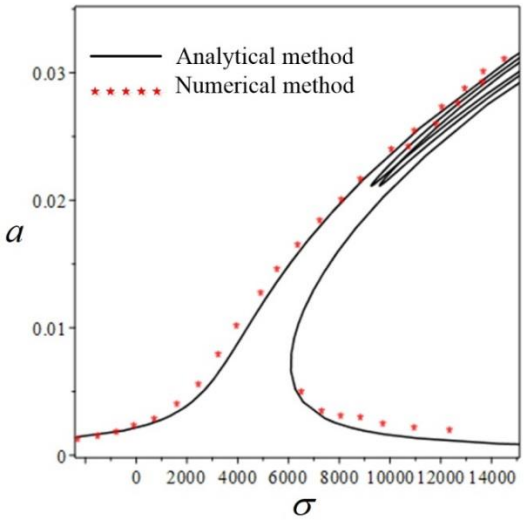

Fig. 3 A comparison between the analytical and numerical frequency response curves ($\theta = 0°, \beta = 90°, K_{sh} = K_{st} = 1$). The amplitude is in meters

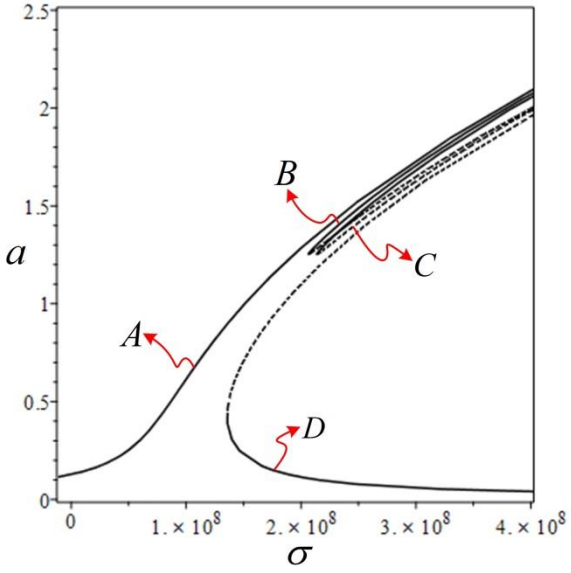

Fig. 4 Frequency response curves of the multilayer FG cylindrical shell without the stiffeners ($K_{sh} = K_{st} = 1$)

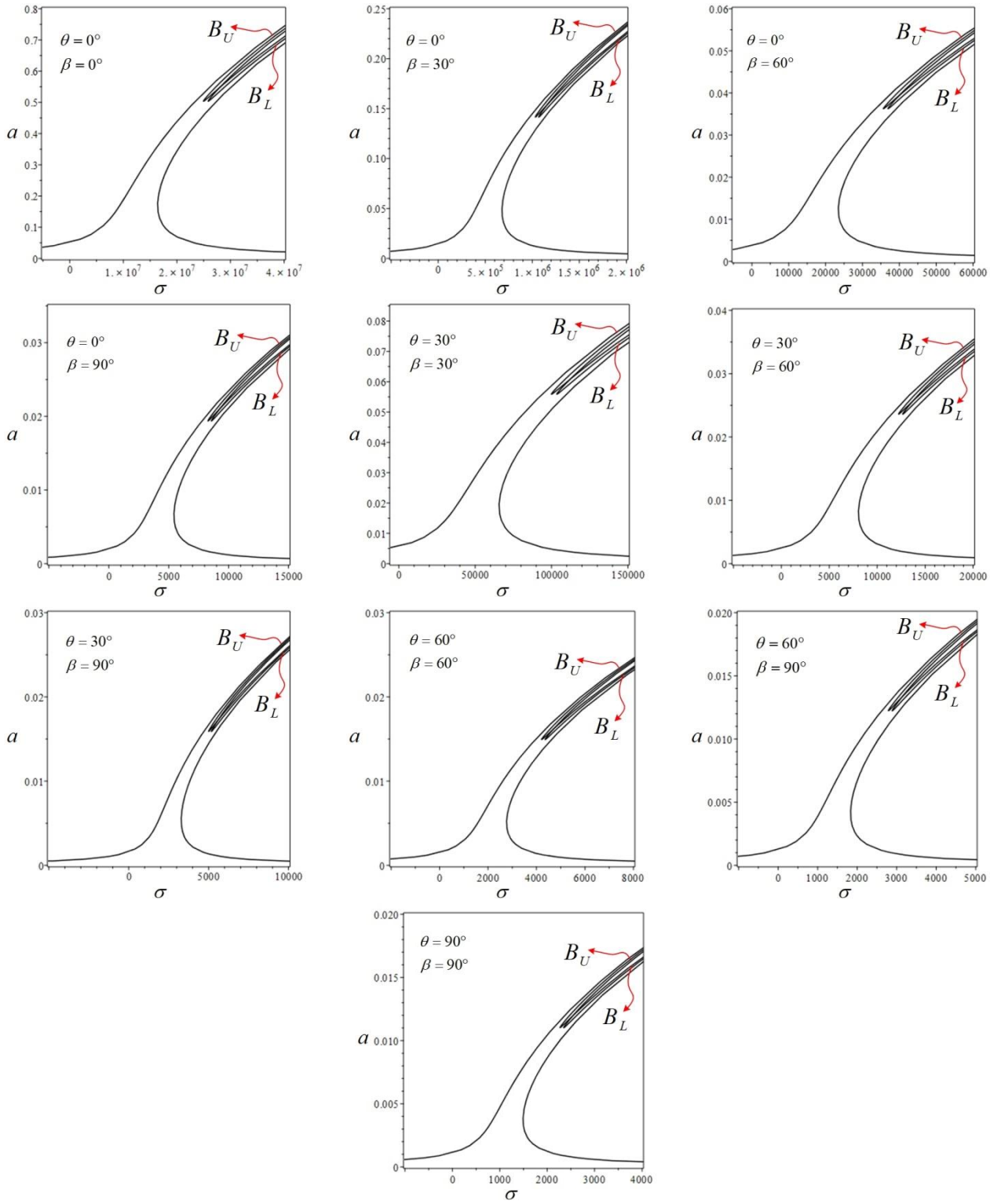

Fig. 5 Frequency response curves of the internal SSMFG cylindrical shell ($K_{sh} = K_{st} = 1$)

Regarding these figures, for the multilayer FG cylindrical shell with internal and external stiffeners, when the angle of stiffeners, i.e., θ and β (Fig. 1) are between 30° and 60° and θ and β are 30°, respectively, the two branches (upper branch (B_U) and lower branch (B_L)) are close together, whereas, when the angle of stiffeners are between 30° and 90° and θ and β are 60° for the internal and external stiffeners, respectively, the two branches are getting distance from together. Also, as can be seen, the hardening nonlinearity behavior of the system with internal and external stiffeners, respectively, is more than other cases when the angles of stiffener are 60° and θ and β are between 30° and 60°, whereas, the hardening nonlinearity behavior of the system with internal and

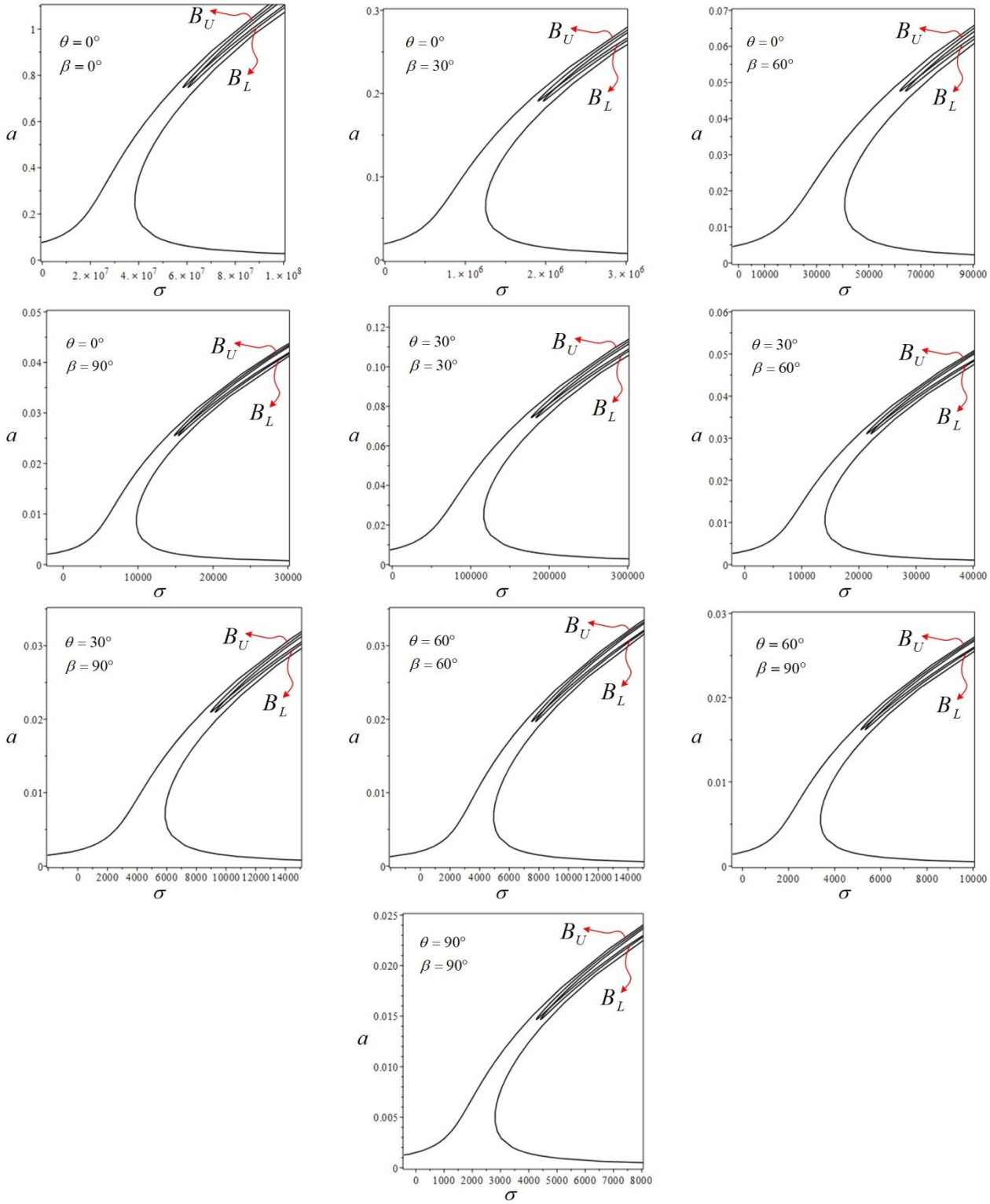

Fig. 6 Frequency response curves of the external SSMFG cylindrical shell ($K_{sh} = K_{st} = 1$)

external stiffeners is less than other cases when the stiffener angles are 0°.

Figs. 7 and 8 illustrate the effect of the shell layers thickness on the response of the amplitude-frequency for the SSMFG cylindrical shell. Regarding these figures, by increasing the thickness of the ceramic and metal layer, the two branches are getting distance from together. Also, as can be seen, by increasing the thickness of the ceramic layer, the hardening nonlinearity behavior of the system is increased. But, by increasing the thickness of the metal layer, the hardening nonlinearity behavior of the system is decreased.

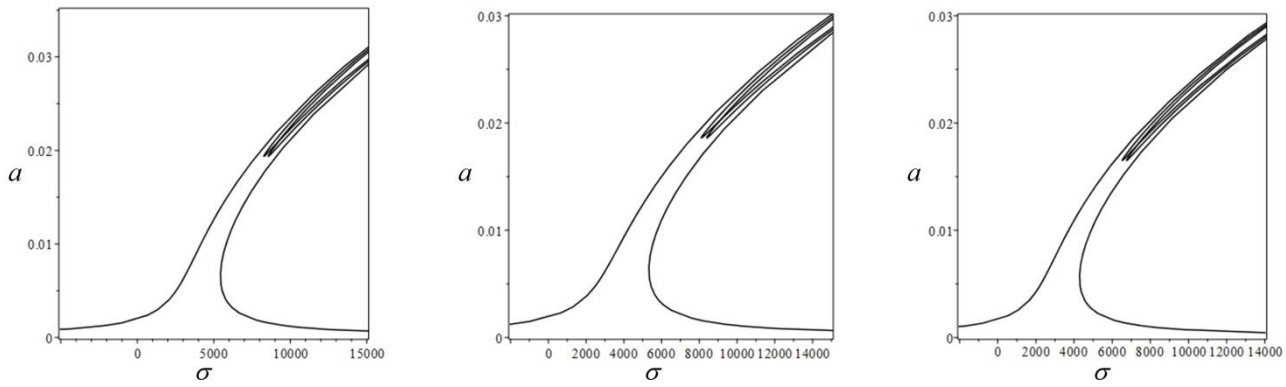

(a) $h_m = 0.012, h_u = 0.004, h_b = 0.004$ (b) $h_m = 0.008, h_u = 0.008, h_b = 0.004$ (c) $h_m = 0.004, h_u = 0.012, h_b = 0.004$

Fig. 7 Effect of thickness of ceramic layer of shell on the frequency response curves of the internal SSMFG cylindrical shells ($\theta = 0°, \beta = 90°, K_{sh} = K_{st} = 1$)

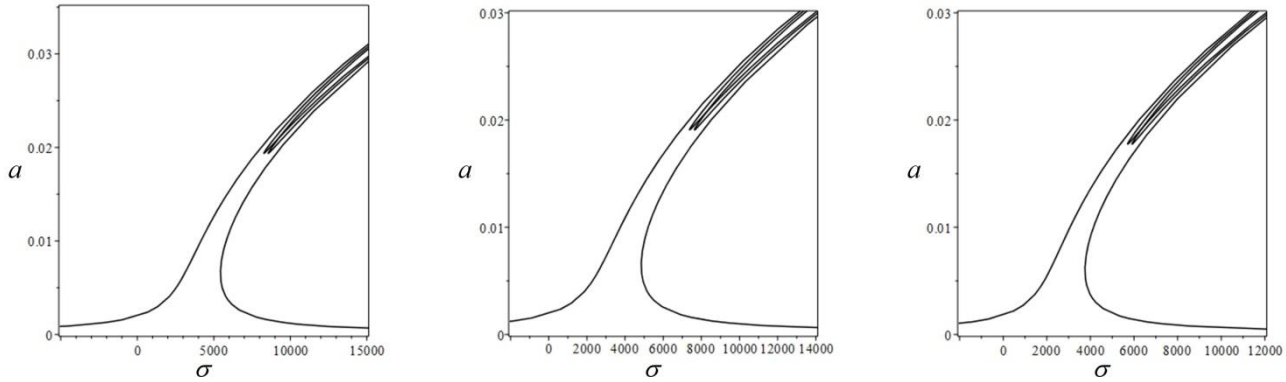

(a) $h_m = 0.012, h_u = 0.004, h_b = 0.004$ (b) $h_m = 0.008, h_u = 0.004, h_b = 0.008$ (c) $h_m = 0.004, h_u = 0.004, h_b = 0.012$

Fig. 8 Effect of thickness of metal layer of shell on the frequency response curves of the internal SSMFG cylindrical shells ($\theta = 0°, \beta = 90°, K_{sh} = K_{st} = 1$)

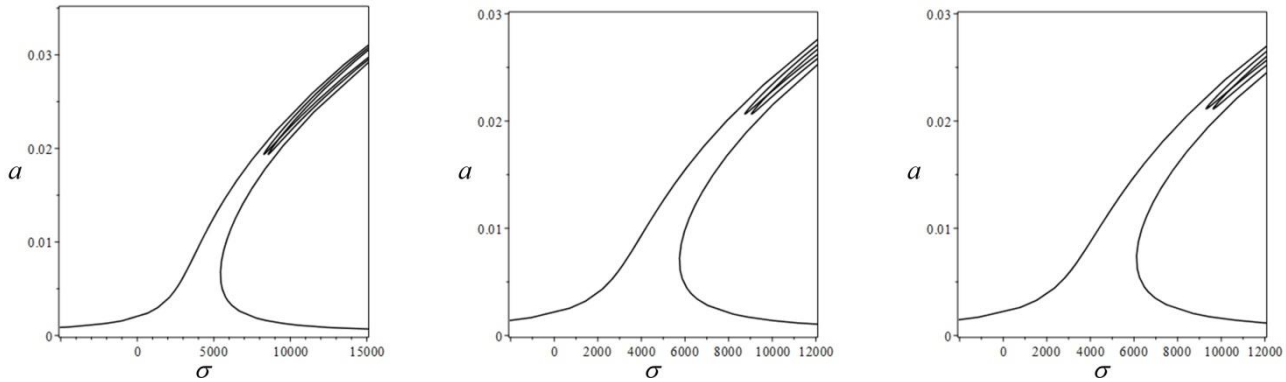

(a) Without elastic foundation (b) Linear elastic foundation (c) Nonlinear elastic foundation

Fig. 9 Effect of elastic foundation on the frequency response curves of the internal SSMFG cylindrical shells ($\theta = 0°, \beta = 90°, K_{sh} = K_{st} = 1$)

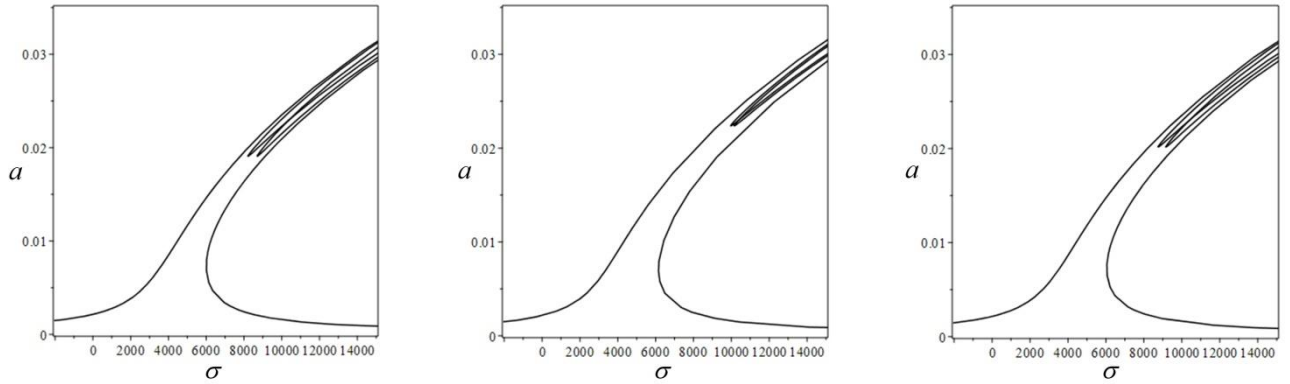

(a) $\theta_2 = 0$ (b) $\theta_2 = \pi$ (c) $\theta_2 = 2\pi$

Fig. 10 Influence of the relative phase of the excitations on the response of the system ($\theta = 0°, \beta = 90°, K_{sh} = K_{st} = 1, \theta_1 = 0$)

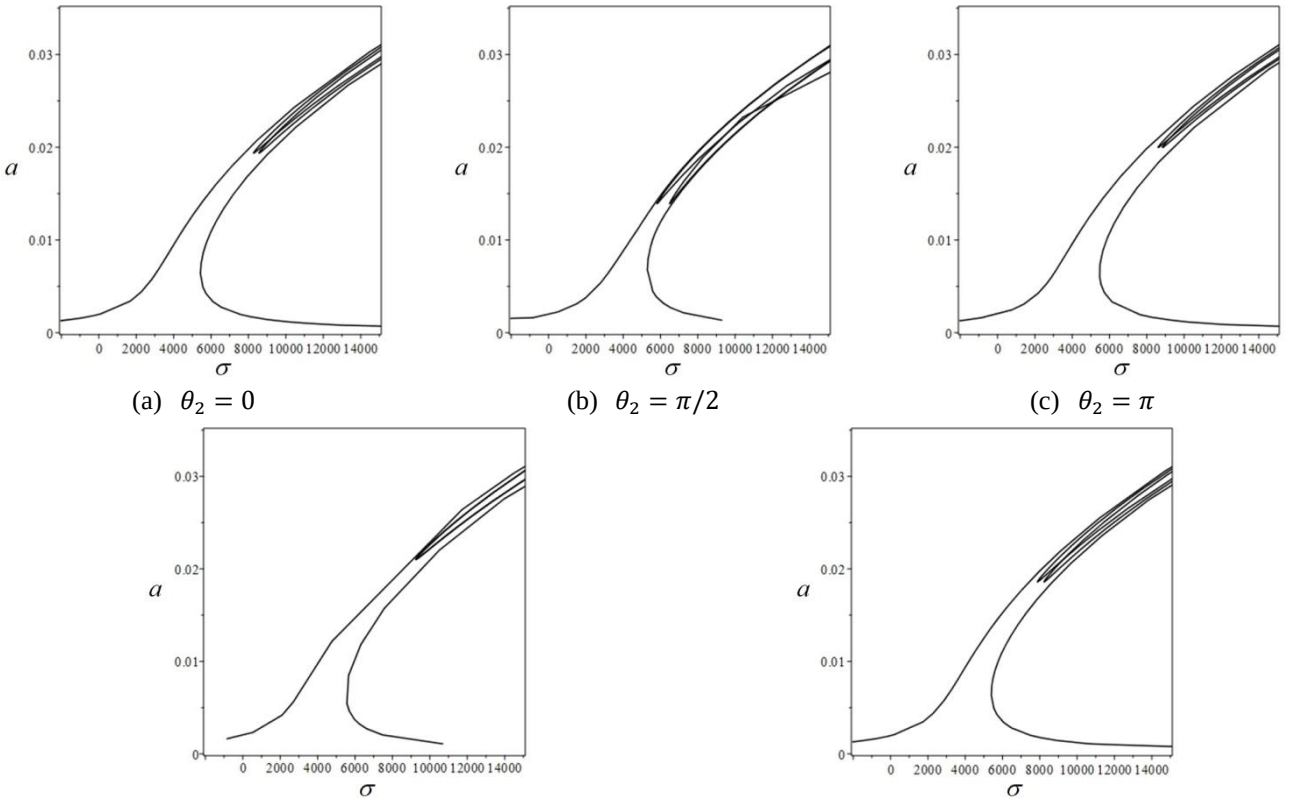

(a) $\theta_2 = 0$ (b) $\theta_2 = \pi/2$ (c) $\theta_2 = \pi$

(d) $\theta_2 = 3\pi/2$ (e) $\theta_2 = 2\pi$

Fig. 11 Influence of the relative phase of the excitations on the response of the system ($\theta = 0°, \beta = 90°, K_{sh} = K_{st} = 1, \theta_1 = \pi/2$)

The effect of elastic foundation on the response of the amplitude-frequency for the SSMFG cylindrical shells is illustrated in Fig. 9. According to this figure, considering the elastic foundation on the system leads to increasing the hardening nonlinearity behavior of the system, and also the two branches are close together. It can be seen, the hardening nonlinearity behavior of the SSMFG cylindrical shells with the nonlinear elastic foundation is more than the hardening nonlinearity behavior of the SSMFG cylindrical shells with linear elastic foundation.

Figs. 10-12 show the influence of the relative phase ($\theta_1 - \theta_2$) of the two excitations on the response of the SSMFG cylindrical shells. This relative phase has only a slight effect on the superharmonic resonance type of curves (branches A and D that is shown in Fig. 4), but it has a significant effect on the subharnonic resonance type of curves (branches B and C that is shown in Fig. 4). In Fig. 10 which θ_1 is equal to 0, as θ_2 increases from 0 to 2π, curves B and C are shifted to the right, while curve C is shifted upward and curve B is shifted downward until they

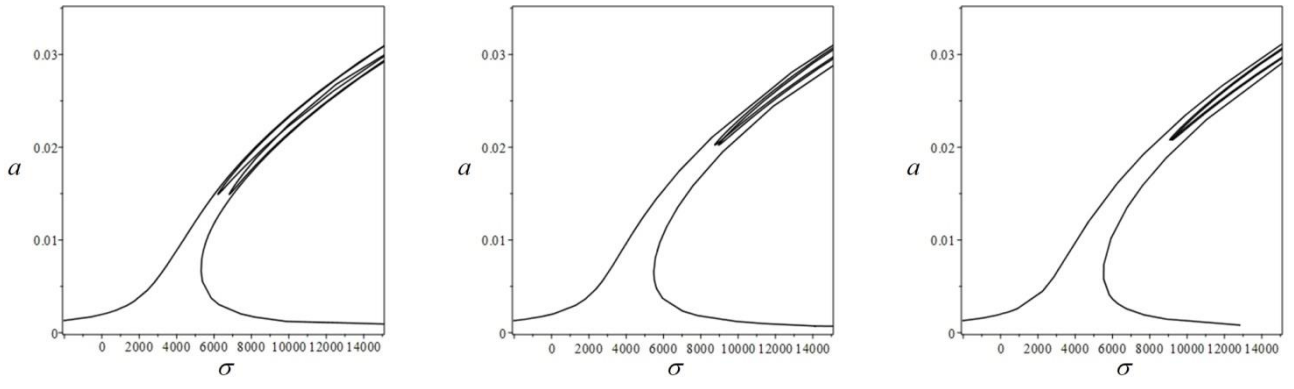

(a) $\theta_2 = 0$ (b) $\theta_2 = \pi/2$ (c) $\theta_2 = \pi$

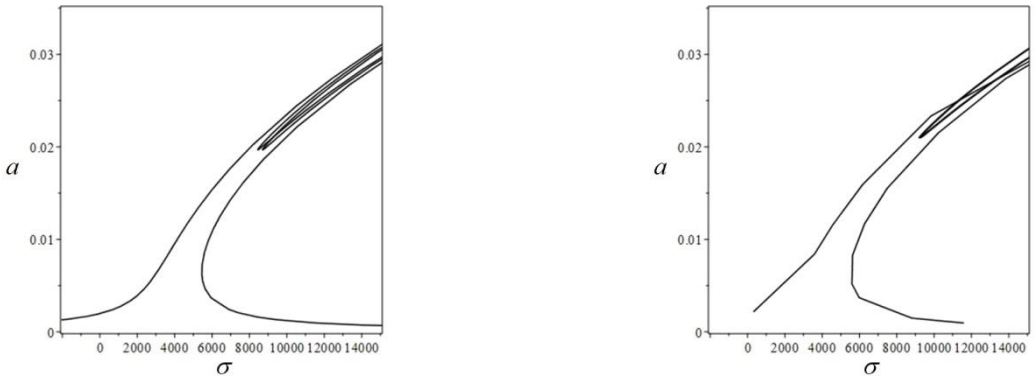

(d) $\theta_2 = 3\pi/2$ (e) $\theta_2 = 2\pi$

Fig. 12 Influence of the relative phase of the excitations on the response of the system ($\theta = 0°, \beta = 90°, K_{sh} = K_{st} = 1, \theta_1 = \pi$)

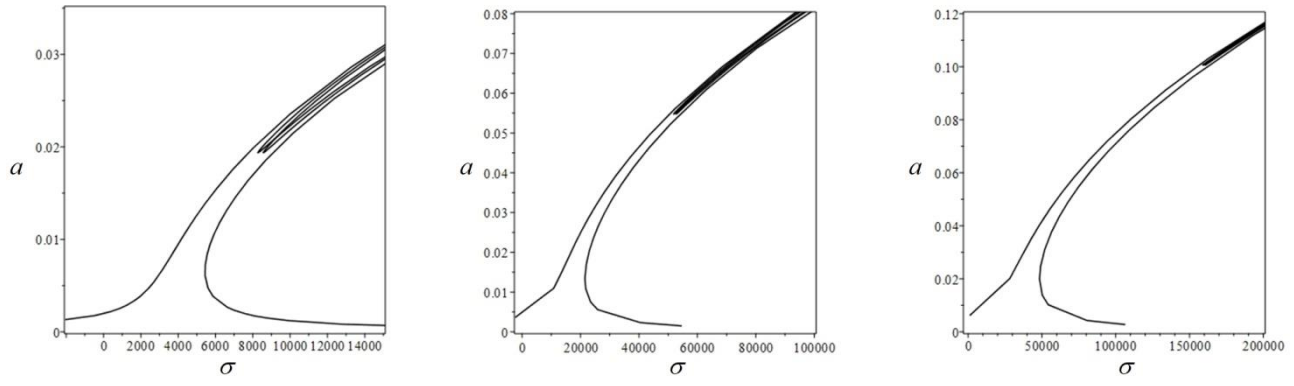

(a) $k_1 = k_2$ (b) $k_1 = 2k_2$ (c) $k_1 = 3k_2$

Fig. 13 Influence of the first amplitude excitation on the frequency response of the system ($\theta = 0°, \beta = 90°$, $K_{sh} = K_{st} = 1$)

are nested when $\theta_2 = \pi$. As θ_2 increases further, the upward and downward shift of curves B and C continues; in addition, they shift to the left. When $\theta_2 = 2\pi$, the frequency response curves are the same as the case $\theta_2 = 0$, except that curves B and C are interchanged. In Fig. 11 which θ_1 is equal to $\pi/2$, when $\theta_2 = \pi/2$, the frequency response curves are the same as the case $\theta_2 = 3\pi/2$, except that curves B and C are getting distance from together. Also, when $\theta_2 = 2\pi$, the frequency response curves are the same as the case $\theta_2 = 0, \pi$, except that curves B and C are interchanged. In Fig. 12 which θ_1 is equal to $3\pi/2$, When $\theta_2 = 3\pi/2$, the frequency response curves are the same as the case $\theta_2 = 0, \pi, \pi/2$ and $3\pi/2$, except that curves B and C are interchanged and when $\theta_2 = 3\pi/2$, the curves B and C are getting close together.

Figs. 13 and 14 illustrate the effect of the load amplitudes of two-term excitation on the frequency response curves of the SSMFG cylindrical shell. According

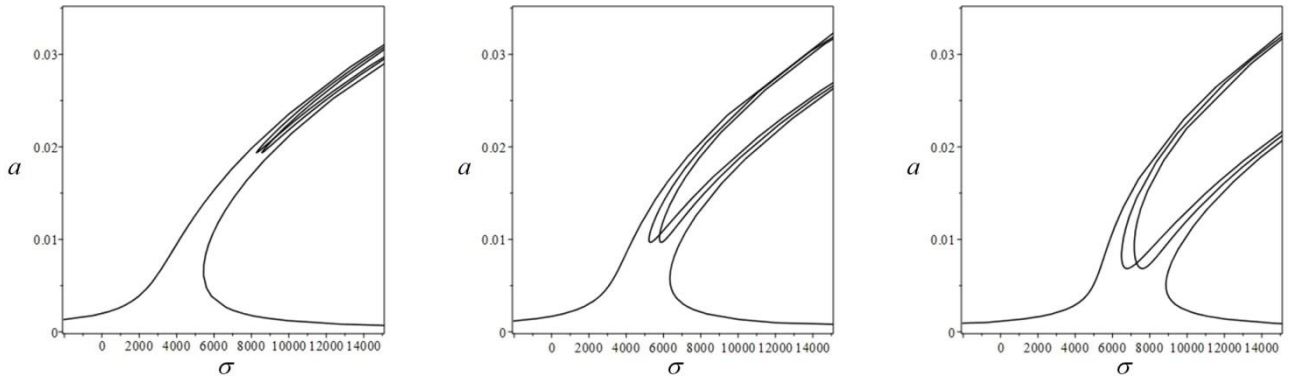

(a) $k_2 = k_1$ (b) $k_2 = 4k_1$ (c) $k_2 = 8k_1$

Fig. 14 Influence of the second amplitude excitation on the frequency response of the system ($\theta = 0°, \beta = 90°, K_{sh} = K_{st} = 1$)

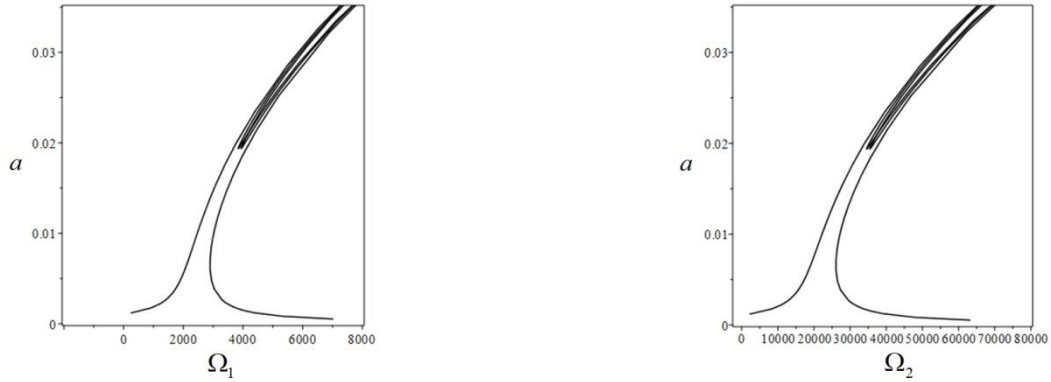

Fig. 15 The curve of amplitude-frequency excitation for the SSMFG cylindrical shell ($\theta = 0°, \beta = 90°, K_{sh} = K_{st} = 1$)

Fig. 13, by increasing the first amplitude excitation (k_1), the two branches are close together. Also, as can be seen, by increasing the value of k_1, the peak amplitudes of the SSMFG cylindrical shell decreases. Whereas, according to Fig. 14, by increasing the second amplitude excitation (k_2), the two branches are getting distance from together. Also, as can be seen, by increasing k_2, upper branch, which is related to superharmonic resonance and is belong to first excitation at constant value of k_1, is fixed and the peak of the lower branch decreases, which is related to subharmonic resonance and is belong to second excitation for different value of k_2.

The curves of amplitude-frequency for the two-term excitation of SSMFG cylindrical shell are shown in Fig. 15. Reg

arding this figure, amplitude excitation responses versus the first and second frequencies of excitation are plotted. As we expected, for a specific value of amplitude, the frequency of the second excitation is nine times of the frequency of the first excitation. This subject is also verified by two relations: $\Omega_1 = \frac{1}{3}(\omega_{mn} + \epsilon\sigma)$ and $\Omega_2 = 3(\omega_{mn} + \epsilon\sigma)$.

6.2 Comprehensive parametric studies on the simultaneous resonances with internal resonance

Similar to the previous sub-section, Eq. (23) has been solved via the fourth-order Runge-Kutta procedure. In this method, the maximum amplitude has been detected for various magnitudes of the excitation, based on the time responses, using the initial conditions $W(0) = 0$ and $\dot{W}(0) = 0$. So, according to this explanation, the numerical frequency response curves for the four prominent order modes are plotted in Fig. 16. As can be seen, the frequency response curve of mode 3 is approximately like the mode 4.

The influence of stiffeners angle on the nonlinear vibration behavior and the phase portrait of nonlinear vibration of SSMFG cylindrical shell with simultaneous resonances and 1:1:3:3 internal resonances for the four prominent order modes is demonstrated in Figs. 17-19. Regarding the obtained results, it can be seen that the effects of stiffeners angle among 60° and 90° are more than other stiffeners angle. Also, according to these figures, the phase portrait curve of the SSMFG cylindrical shell becomes more disorderly, when the stiffeners angle $\theta = \beta = 0^\circ$. Furthermore, the vibration amplitude of shells with the stiffeners angle $\theta = \beta = 90^\circ$ is less than others. Also, the nonlinear vibration behavior and the phase portrait of

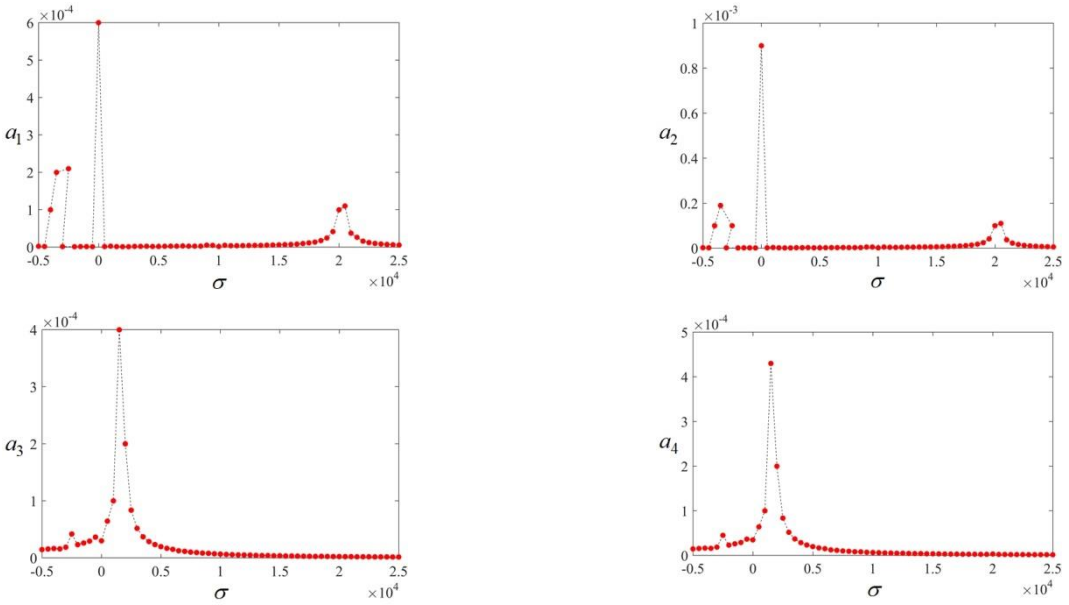

Fig. 16 The frequency response curves for the four prominent order modes of the system

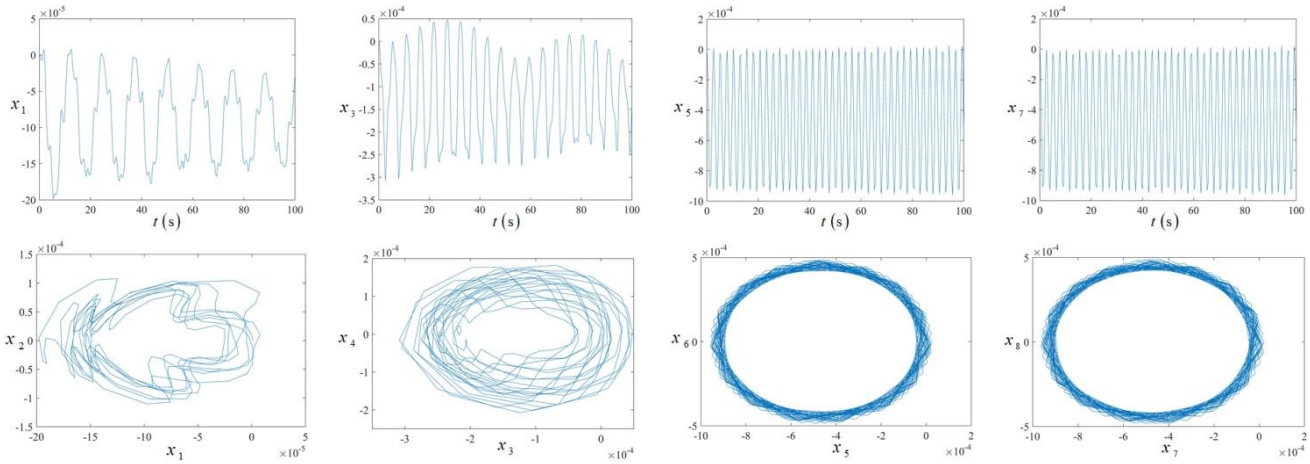

Fig. 17 The nonlinear vibration responses of SSMFG cylindrical shell ($\theta = 0°, \beta = 0°, K_{sh} = K_{st} = 1$)

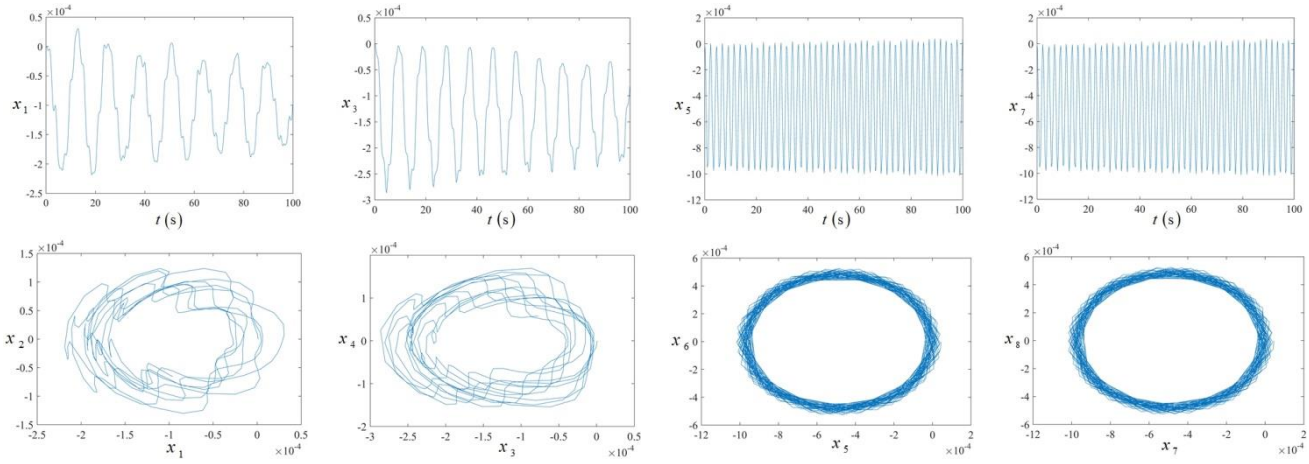

Fig. 18 The nonlinear vibration responses of SSMFG cylindrical shell ($\theta = 60°, \beta = 60°, K_{sh} = K_{st} = 1$)

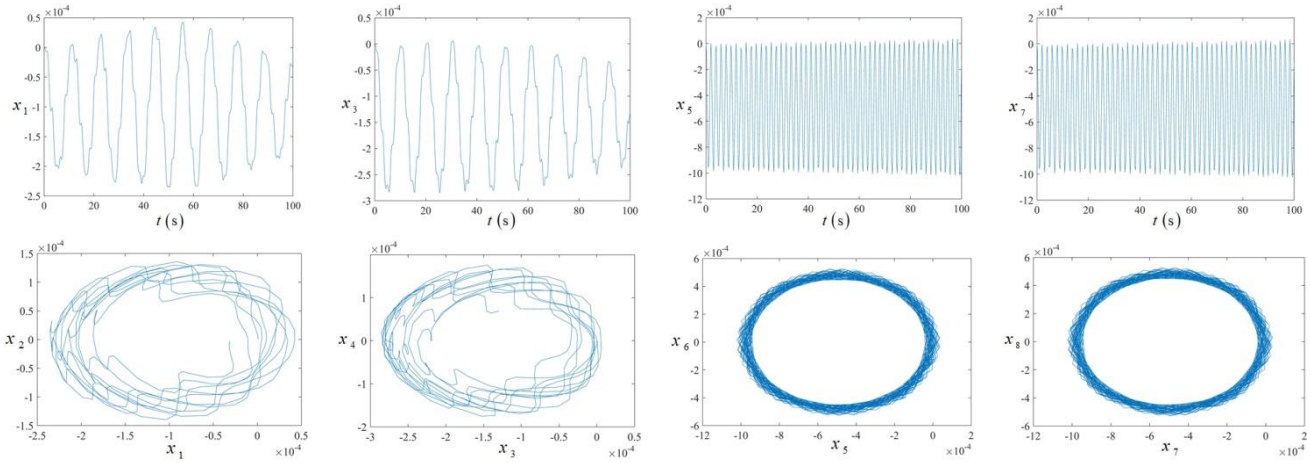

Fig. 19 The nonlinear vibration responses of SSMFG cylindrical shell ($\theta = 90°, \beta = 90°, K_{sh} = K_{st} = 1$)

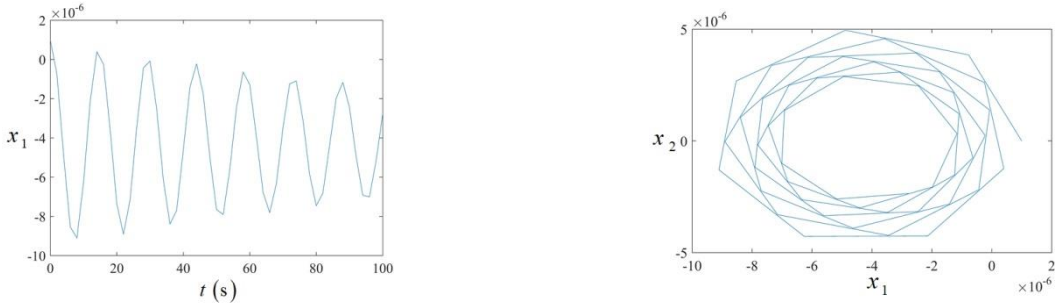

Fig. 20 The nonlinear vibration responses of SSMFG cylindrical shell for the single mode ($\theta = 60°, \beta = 60°, K_{sh} = K_{st} = 1$)

nonlinear vibration of SSMFG cylindrical shell for the single mode are illustrated in Fig 20. As can be seen, the behavior of the curves for the single mode is different with the multi modes, but the trend of the curves for the single mode approximately like the multi modes that this is due to the effect of modes on the internal resonance.

7. Conclusions

A semi-analytical approach is developed to investigate the simultaneous resonance of a spiral stiffened multilayer cylindrical shell with FG material resting on Winkler-Pasternak-Kelvin-Voigt viscoelastic foundations with cubic nonlinear stiffness, under two-term harmonic excitations. The cylindrical shell has three layers consist of ceramic, FGM, and metal. The exterior layer of the cylindrical shell is rich ceramic while the interior layer is rich metal and the functionally graded material layer is located between these layers. The material distribution of the stiffeners was graded in the thickness direction. von Kármán-type of kinematic nonlinearity was adopted to enable large deformations analyses. Then, the coupled nonlinear response of the problem was obtained using the concept of stress function, Galerkin's orthogonality, and the smeared stiffeners technique. To determine the system response for the simultaneous resonances, the multiple scales method was utilized. Then, the influences of various material, geometric, loading, and foundation parameters were investigated. Some of the main conclusions may be summarized in the following form:

- For the multilayer FG cylindrical shell with internal and external stiffeners, when the angle of stiffeners (θ and β) are between 30° and 60° and θ and β are 30°, respectively, the two branches are close together, whereas, when the angle of stiffeners are between 30° and 90° and θ and β are 60° for the internal and external stiffeners, respectively, the two branches are getting distance from together.
- The hardening nonlinearity behavior of the system with internal and external stiffeners, respectively, is more than other cases when the angles of stiffener are 60° and θ and β are between 30° and 60°, whereas, the hardening nonlinearity behavior of the system with internal and external stiffeners is less than other cases when the stiffener angles are 0°.
- By increasing the thickness of the ceramic and metal layer, the two branches are getting distance from together. Also, as can be seen, by increasing the thickness of the ceramic layer, the hardening nonlinearity behavior of the system is increased. But, by increasing the thickness of the metal layer,

the hardening nonlinearity behavior of the system is decreased.

- Considering the elastic foundation on the system leads to increasing the hardening nonlinearity behavior of the system, and also the two branches are close together.
- The hardening nonlinearity behavior of the SSMFG cylindrical shells with the nonlinear elastic foundation is more than the hardening nonlinearity behavior of the SSMFG cylindrical shells with a linear elastic foundation.
- By increasing the first amplitude excitation, the two branches are getting near together and the peak amplitudes of the SSMFG cylindrical shell decreases.
- By increasing the second amplitude excitation, the two branches are getting distance from together and upper branch is fixed, whereas the peak of the lower branch decreases.
- The phase portrait curve of the SSMFG cylindrical shell becomes more disorderly, when the stiffeners angle $\theta = \beta = 0^{\circ}$.
- The vibration amplitude of shells with the stiffeners angle $\theta = \beta = 90^{\circ}$ is less than others.

References

Abe, A., Kobayashi, Y. and Yamada, G. (2007), "Nonlinear dynamic behaviors of clamped laminated shallow shells with one-to-one internal resonance", *J. Sound Vib.*, **304**, 957-968. https://doi.org/10.1016/j.jsv.2007.03.009.

Ahmadi, H. (2018), "Nonlinear primary resonance of imperfect spiral stiffened functionally graded cylindrical shells surrounded by damping and nonlinear elastic foundation", *Eng. Comput.*, 1-15. https://doi.org/10.1007/s00366-018-0679-2.

Ahmadi, H. and Foroutan, K. (2019a), "Superharmonic and subharmonic resonances of spiral stiffened functionally graded cylindrical shells under harmonic excitation", *Int. J. Struct. Stab. Dyn*., https://doi.org/10.1142/S0219455419501141.

Ahmadi, H. and Foroutan, K. (2019b), "Nonlinear primary resonance of spiral stiffened functionally graded cylindrical shells with damping force using the method of multiple scales", *Thin Wall. Struct.*, **135**, 33-44. https://doi.org/10.1016/j.tws.2018.10.028.

Ahmadi, H. and Foroutan, K. (2019c), "Combination resonance analysis of FG porous cylindrical shell under two-term excitation", *Steel Compos. Struct*., **32**(2), 253-264. https://doi.org/10.12989/scs.2019.32.2.253.

Alijani, F., Amabili, M. and Bakhtiari-Nejad, F. (2011), "On the accuracy of the multiple scales method for non-linear vibrations of doubly curved shallow shells", *Int. J. Nonlinear. Mech.*, **46**, 170-179. https://doi.org/10.1016/j.ijnonlinmec.2010.08.006.

Bich, D.H., Van Dung, D., Nam, V.H. and Phuong, N.T. (2013), "Nonlinear static and dynamic buckling analysis of imperfect eccentrically stiffened functionally graded circular cylindrical thin shells under axial compression", *Int. J. Mech. Sci.*, **74**, 190-200. https://doi.org/10.1016/j.ijmecsci.2013.06.002.

Dai, H.L., Dai, T. and Zheng, H.Y. (2013), "Creep buckling and post-buckling analyses for a hybrid laminated viscoelastic FGM cylindrical shell under in-plane loading", *Int. J. Mech. Mater. Des.*, **9**(4), 309-323. https://doi.org/10.1007/s10999-013-9223-0.

Dat, N.D., Quan, T.Q. and Duc, N.D. (2019), "Nonlinear thermal vibration of carbon nanotube polymer composite elliptical cylindrical shells", *Int. J. Mech. Mater. Des.*, 1-20. https://doi.org/10.1007/s10999-019-09464-y.

Du, C. and Li, Y. (2013), "Nonlinear resonance behavior of functionally graded cylindrical shells in thermal environments", *Compos. Struct.*, **102**, 164-174. https://doi.org/10.1016/j.compstruct.2013.02.028.

Duc, N.D., Thang, P.T. (2015), "Nonlinear dynamic response and vibration of shear deformable imperfect eccentrically stiffened S-FGM circular cylindrical shells surrounded on elastic foundations", *Aerosp. Sci. Technol.*, **40**, 115-127.

Ebrahimi, F. and Habibi, S. (2016), "Deflection and vibration analysis of higher-order shear deformable compositionally graded porous plate", *Steel Compos. Struct.*, **20**(1), 205-225. http://dx.doi.org/10.12989/scs.2016.20.1.205.

Foroutan, K., Shaterzadeh, A. and Ahmadi, H. (2018), "Nonlinear dynamic analysis of spiral stiffened functionally graded cylindrical shells with damping and nonlinear elastic foundation under axial compression", *Struct. Eng. Mech.*, **66**(3), 295-303. https://doi.org/10.12989/sem.2018.66.3.295.

Foroutan, K. and Ahmadi, H. (2020), "Nonlinear free vibration analysis of SSMFG cylindrical shells resting on nonlinear viscoelastic foundation in thermal environment", *Appl. Math. Model.*, **85**, 294-317. https://doi.org/10.1016/j.apm.2020.04.017.

Foroutan, K., Shaterzadeh, A. and Ahmadi, H. (2019), "Nonlinear dynamic analysis of spiral stiffened cylindrical shells rested on elastic foundation", *Steel Compos. Struct.*, **32**(4), 509-519. https://doi.org/10.12989/scs.2019.32.4.509.

Gao, K., Gao, W., Chen, D. and Yang, J. (2018a), "Nonlinear free vibration of functionally graded graphene platelets reinforced porous nanocomposite plates resting on elastic foundation", *Compos. Struct.*, **204**, 831-846. https://doi.org/10.1016/j.compstruct.2018.08.013.

Gao, K., Gao, W., Wu, D. and Song, C. (2017), "Nonlinear dynamic characteristics and stability of composite orthotropic plate on elastic foundation under thermal environment", *Compos. Struct.*, **168**, 619-632. https://doi.org/10.1016/j.compstruct.2017.02.054.

Gao, K., Gao, W., Wu, D. and Song, C. (2018b), "Nonlinear dynamic stability of the orthotropic functionally graded cylindrical shell surrounded by Winkler-Pasternak elastic foundation subjected to a linearly increasing load", *J. Sound Vib.*, **415**, 147-168. https://doi.org/10.1016/j.jsv.2017.11.038.

Khayat, M., Dehghan, S.M., Najafgholipou,r M.A. and Baghlani, A. (2018), "Free vibration analysis of functionally graded cylindrical shells with different shell theories using semi-analytical method", *Steel Compos. Struct.*, **28**(6), 735-748. https://doi.org/10.12989/scs.2018.28.6.735

Javed, S., Viswanathan, K.K. and Aziz, Z.A. (2016), "Free vibration analysis of composite cylindrical shells with non-uniform thickness walls", *Steel Compos. Struct.*, **20**(5), 1087-1102. https://dx.doi.org/10.12989/scs.2016.20.5.1087.

Lezgy-Nazargah, M., Shariyat, M. and Beheshti-Aval, S.B. (2011), "A refined high-order global-local theory for finite element bending and vibration analyses of the laminated composite beams", *Acta Mech.*, **217**(3-4), 219-242. https://doi.org/10.1007/s00419-012-0621-9.

Li, F.M. and Yao, G. (2013), "1/3 Subharmonic resonance of a nonlinear composite laminated cylindrical shell in subsonic air flow", *Compos. Struct.*, **100**, 249-256. https://doi.org/10.1016/j.compstruct.2012.12.035.

Li, X., Du, C.C. and Li, Y.H. (2018), "Parametric resonance of a FG cylindrical thin shell with periodic rotating angular speeds in thermal environment", *Appl. Math. Model.*, **59**, 393-409. https://doi.org/10.1016/j.apm.2018.01.048.

Mahmoudkhani, S., Navazi, H.M. and Haddadpour, H. (2011), "An analytical study of the non-linear vibrations of cylindrical

shells", *Int. J. Nonlinear. Mech.*, **46**, 1361-1372. https://doi.org/10.1016/j.ijnonlinmec.2011.07.012.

Mustafa, B.A.J. and Ali, R. (1989), "An energy method for free vibration analysis of stiffened circular cylindrical shells", *Comput. Struct.*, **32**, 355-363. https://doi.org/10.1016/0045-7949(89)90047-3.

Nam, V.H., Phuong, N.T., Van Minh, K. and Hieu, P.T. (2018), "Nonlinear thermo-mechanical buckling and post-buckling of multilayer FGM cylindrical shell reinforced by spiral stiffeners surrounded by elastic foundation subjected to torsional loads", *Eur. J. Mech. A-Solid.*, **72**, 393-406. https://doi.org/10.1016/j.euromechsol.2018.06.005.

Nayfeh, A.H. and Mook D.T. (1995), *Nonlinear Oscilations*, John Wiley and Sons.

Pendhari, S.S., Kant, T., Desai, Y.M. and Subbaiah, C.V. (2012), "Static solutions for functionally graded simply supported plates", *Int. J. Mech. Mater. Des.*, **8**(1), 51-69. https://doi.org/10.1007/s10999-011-9175-1.

Pellicano F. (2007), "Vibrations of circular cylindrical shells: theory and experiments", *J. Sound Vib.*, **303**(1-2), 154-170. https://doi.org/10.1016/j.jsv.2007.01.022.

Qin, Z. Chu, F. and Zu, J. (2017), "Free vibrations of cylindrical shells with arbitrary boundary conditions: A comparison study", *Int. J. Mech. Sci.*, **133** 91-99. https://doi.org/10.1016/j.ijmecsci.2017.08.012.

Rodrigues, L., Gonçalves, P.B. and Silva, F.M.A. (2017), "Internal resonances in a transversally excited imperfect circular cylindrical shell", *Pro. Eng.*, **199**, 838-843. https://doi.org/10.1016/j.proeng.2017.09.010.

Sarigul, M. and Boyaci, H. (2010), "Nonlinear vibrations of axially moving beams with multiple concentrated masses Part I: primary resonance", *Struct. Eng. Mech.*, **36**(2), 149-163. https://doi.org/10.12989/sem.2010.36.2.149.

Shaterzadeh, A. and Foroutan, K. (2016), "Post-buckling of cylindrical shells with spiral stiffeners under elastic foundation", *Struct. Eng. Mech.*, **60**, 615-631. https://doi.org/10.12989/sem.2016.60.4.615.

Sheng, G.G. and Wang, X. (2018a), "Nonlinear vibrations of FG cylindrical shells subjected to parametric and external excitations", *Compos. Struct.*, **191**, 78-88. https://doi.org/10.1016/j.compstruct.2018.02.018.

Sheng, G.G. and Wang, X. (2018b), "The dynamic stability and nonlinear vibration analysis of stiffened functionally graded cylindrical shells", *Appl. Math. Model.*, **56**, 389-403.
https://doi.org/10.1016/j.apm.2017.12.021.

Sofiyev, A.H. (2016), "Large amplitude vibration of FGM orthotropic cylindrical shells interacting with the nonlinear Winkler elastic foundation", *Compos. Part B*, **98**, 141-50. https://doi.org/10.1016/j.compositesb.2016.05.018.

Sofiyev, A.H., Avcar, M., Ozyigit, P. and Adigozel, S. (2009), "The Free Vibration of non-homogeneous truncated conical shells on a winkler foundation", *Int. J. Eng. Appl. Sci.*, **1**, 34-41.

Sofiyev, A.H., Hui, D., Haciyev, V.C., Erdem, H., Yuan, G.Q., Schnack, E. and Guldal, V. (2017), "The nonlinear vibration of orthotropic functionally graded cylindrical shells surrounded by an elastic foundation within first order shear deformation theory", *Compos. Part B*, **116**, 170-85. https://doi.org/10.1016/j.compositesb.2017.02.006.

Van Dung, D. and Hoa, L.K. (2013), "Nonlinear buckling and post-buckling analysis of eccentrically stiffened functionally graded circular cylindrical shells under external pressure", *Thin Wall. Struct.*, **63**,117-124. https://doi.org/10.1016/j.tws.2012.09.010.

Van Dung, D. and Nam, V.H. (2014), "Nonlinear dynamic analysis of eccentrically stiffened functionally graded circular cylindrical thin shells under external pressure and surrounded by an elastic medium", *Eur. J. Mech. A-Solid.*, **46** 42-53. https://doi.org/10.1016/j.euromechsol.2014.02.008.

Wang, Y.Q. (2018), "Electro-mechanical vibration analysis of functionally graded piezoelectric porous plates in the translation state", *Acta Astronaut.*, **143**, 263-271. https://doi.org/10.1016/j.actaastro.2017.12.004.

Wang, Y.Q. (2014), "Nonlinear vibration of a rotating laminated composite circular cylindrical shell: traveling wave vibration", *Nonlinear Dynam.*, **77**(4), 1693-1707. https://doi.org/10.1007/s11071-014-1410-5.

Wang, Y.Q., Huang, X.B. and Li, J. (2016), "Hydroelastic dynamic analysis of axially moving plates in continuous hot-dip galvanizing process", *Int. J.Mech. Sci.*, **110**, 201-216. https://doi.org/10.1016/j.ijmecsci.2016.03.010.

Wang, Y.Q., Li, H.H., Zhang, Y.F. and Zu, J.W. (2018a), "A nonlinear surface-stress-dependent model for vibration analysis of cylindrical nanoscale shells conveying fluid", *Appl. Math. Model.*, **64**, 55-70. https://doi.org/10.1016/j.apm.2018.07.016.

Wang, Y.Q., Liang, L. and Guo, X.H. (2013), "Internal resonance of axially moving laminated circular cylindrical shells", *J. Sound Vib.*, **332**, 6434-6450. https://doi.org/10.1016/j.jsv.2013.07.007.

Wang, Y.Q., Liu, Y.F. and Yang, T.H. (2019c), "Nonlinear Thermo-Electro-Mechanical Vibration of Functionally Graded Piezoelectric Nanoshells on Winkler–Pasternak Foundations Via Nonlocal Donnell's Nonlinear Shell Theory", *Int. J. Struct. Stab. Dynam.*, **19**(9), 1950100. https://doi.org/10.1142/S0219455419501001.

Wang, Y.Q. and Liu, Y.F. (2019), "Free vibration and buckling of polymeric shells reinforced with 3D graphene foams", *Results in Phys.*, **14**, 102510. https://doi.org/10.1016/j.rinp.2019.102510.

Wang, Y.Q., Ye, C. and Zu, J.W. (2018b), "Identifying the temperature effect on the vibrations of functionally graded cylindrical shells with porosities", *Appl. Math. Mech.*, **39**(11), 1587-1604. https://doi.org/10.1007/s10483-018-2388-6.

Wang, Y.Q., Wan, Y.H. and Zu, J.W. (2019a), "Nonlinear dynamic characteristics of functionally graded sandwich thin nanoshells conveying fluid incorporating surface stress influence", *Thin Wall. Struct.*, **135**, 537-547. https://doi.org/10.1016/j.tws.2018.11.023.

Wang, Y.Q., Wan, Y.H. and Zhang, Y.F. (2017), "Vibrations of longitudinally traveling functionally graded material plates with porosities", *Eur. J. Mech. A-Solid.*, **66**, 55-68. https://doi.org/10.1016/j.euromechsol.2017.06.006.

Wang, Y.Q. and Yang, Z. (2017), "Nonlinear vibrations of moving functionally graded plates containing porosities and contacting with liquid: internal resonance", *Nonlinear Dynam.*, **90**(2), 1461-1480. https://doi.org/10.1007/s11071-017-3739-z.

Wang, Y.Q. and Zhao, H.L. (2019), "Free vibration analysis of metal foam core sandwich beams on elastic foundation using Chebyshev collocation method", *Arch. Appl. Mech.*, **89**(11), 2335-2349. https://doi.org/10.1007/s00419-019-01579-0.

Wang, Y.Q., Ye, C. and Zu, J.W. (2019b), "Nonlinear vibration of metal foam cylindrical shells reinforced with graphene platelets", *Aerosp. Sci. Technol.*, **85**, 359-370. https://doi.org/10.1016/j.ast.2018.12.022.

Wang, Y.Q., Ye, Ch. and Zu, J.W. (2019d), "Vibration analysis of circular cylindrical shells made of metal foams under various boundary conditions", *Int. J. Mech. Mater. Des.*, **15**(2), 333-344.
https://doi.org/10.1007/s10999-018-9415-8.

Wang, Y.Q. and Zu, J.W. (2017a), "Instability of viscoelastic plates with longitudinally variable speed and immersed in ideal liquid," *Int. J. Appl. Mech.*, **9**(1), 1750005. https://doi.org/10.1142/S1758825117500053.

Wang, Y.Q. and Zu, J.W. (2017b), "Porosity-dependent nonlinear forced vibration analysis of functionally graded piezoelectric smart material plates", *Smart Mater. Struct.*, **26**(10), 105014.

https://doi.org/10.1088/1361-665X/aa8429.
Wang, Y.Q. and Zu, J.W. (2017c), "Nonlinear steady-state responses of longitudinally traveling functionally graded material plates in contact with liquid", *Compos. Struct.*, **164**, 130-144. https://doi.org/10.1016/j.compstruct.2016.12.053.
Wang, Y.Q. and Zu, J.W. (2017d), "Vibration behaviors of functionally graded rectangular plates with porosities and moving in thermal environment", *Aerosp. Sci. Technol.*, **69**, 550-562. https://doi.org/10.1016/j.ast.2017.07.023.
Yas, M.H. and Garmsiri, K. (2010), "Three-dimensional free vibration analysis of cylindrical shells with continuous grading reinforcement", *Steel Compos. Struct.*, **10**(4), 349-360. https://doi.org/10.12989/scs.2010.10.4.349.
Zhang, W., Liu, T., Xi, A. and Wang, Y.N. (2018), "Resonant responses and chaotic dynamics of composite laminated circular cylindrical shell with membranes", *J. Sound Vib.*, **423**, 65-99. https://doi.org/10.1016/j.jsv.2018.02.049.
Zarouni, E., Rad, M.J. and Tohidi, H. (2014), "Free vibration analysis of fiber reinforced composite conical shells resting on Pasternak-type elastic foundation using Ritz and Galerkin methods", *Int. J. Mech. Mater. Des.*, **10**(4), 421-438. https://doi.org/10.1007/s10999-014-9254-1 .

CC

Appendix A

The H matrix of Eq. (8) is

$$
\begin{aligned}
H_{11} &= \cos^3 q + \cos^3 b \\
H_{21} &= \sin q \cos^2 q + \sin b \cos^2 b \\
H_{31} &= \cos^2 q - \cos^2 b \\
H_{12} &= \sin^2 q \cos q + \sin^2 b \cos b \\
H_{22} &= \sin^3 q + \sin^3 b \\
H_{32} &= \sin q \cos q + \sin b \cos b \\
H_{13} &= 2\left(\sin q \cos^2 q - \sin b \cos^2 b\right) \\
H_{23} &= 2\left(\sin^2 q \cos q - \sin^2 b \cos b\right) \\
H_{33} &= \sin^2 q - \sin^2 b
\end{aligned}
\tag{A.1}
$$

where

$$
\begin{Bmatrix} h_1 \\ h_2 \\ h_3 \end{Bmatrix} = \frac{h_s dE_s}{s h_s} \sin(\theta + \beta) \begin{Bmatrix} 1/(\sin\theta + \sin\beta) \\ 1/(\cos\theta + \cos\beta) \\ 1/2 \end{Bmatrix} \tag{A.2}
$$

Appendix B

The new parameters of Eqs. (12), (13), (16), and (19) may be defined as (Foroutan *et al.* 2018, Shaterzadeh and Foroutan 2016)

$$A = J_{11}^{*}m^4\pi^4 + (J_{33}^{*} - J_{12}^{*} - J_{21}^{*})m^2n^2\pi^2\lambda^2 + J_{22}^{*}n^4\lambda^4$$

$$B = J_{21}^{**}m^4\pi^4 + (J_{11}^{*} + J_{22}^{*} - 2J_{36}^{**})m^2n^2\pi^2\lambda^2 + J_{12}^{**}n^4\lambda^4 - \frac{L^2}{R}m^2n^2$$

$$B^{*} = A_{21}^{*}m^4\pi^4 + (A_{11}^{*} + A_{22}^{*} - 2J_{36}^{**})m^2n^2\pi^2\lambda^2 + J_{12}^{**}n^4\lambda^4 - \frac{L^2}{R}m^2n^2 \quad \text{(B.1)}$$

$$D = A_{11}^{**}m^4\pi^4 + (A_{12}^{**} + A_{21}^{**} + 4A_{36}^{**})m^2n^2\pi^2\lambda^2 + A_{22}^{**}n^4\lambda^4$$

$$G = \left(\frac{n^4\lambda^4}{16J_{11}^{*}} + \frac{m^4\pi^4}{16J_{22}^{*}}\right), \quad \lambda = \frac{L}{R}$$

where

$$\Delta = J_{11}J_{22} - J_{12}J_{21}, \quad J_{22}^{*} = \frac{J_{22}}{\Delta}, \quad J_{12}^{*} = \frac{J_{12}}{\Delta}$$

$$J_{11}^{*} = \frac{J_{11}}{\Delta}, \quad J_{21}^{*} = \frac{J_{21}}{\Delta}, \quad J_{33}^{*} = \frac{1}{J_{33}}, \quad J_{36}^{*} = \frac{J_{36}}{J_{33}}$$

$$J_{11}^{**} = J_{22}^{*}J_{14} - J_{12}^{*}J_{24}, \quad J_{12}^{**} = J_{22}^{*}J_{15} - J_{12}^{*}J_{25}$$

$$J_{21}^{**} = J_{11}^{*}J_{24} - J_{21}^{*}J_{14}, \quad J_{22}^{**} = J_{11}^{*}J_{25} - J_{21}^{*}J_{15}$$

$$A_{11}^{*} = J_{22}^{*}J_{14} - J_{21}^{*}J_{15}, \quad A_{21}^{*} = J_{11}^{*}J_{15} - J_{12}^{*}J_{14} \quad \text{(B.2)}$$

$$A_{12}^{*} = J_{22}^{*}J_{24} - J_{21}^{*}J_{25}, \quad A_{22}^{*} = J_{11}^{*}J_{25} - J_{12}^{*}J_{24}$$

$$A_{11}^{**} = J_{11}^{**}J_{14} - J_{21}^{**}J_{15} - J_{41}, \quad A_{12}^{**} = J_{12}^{**}J_{14} - J_{22}^{**}J_{15} - J_{42}$$

$$A_{21}^{**} = J_{11}^{**}J_{24} - J_{21}^{**}J_{25} - J_{51}, \quad A_{22}^{**} = J_{12}^{**}J_{24} - J_{22}^{**}J_{25} - J_{52}$$

$$A_{36}^{**} = J_{36}^{**}J_{36} - J_{63}$$

and

$$J_{12} = \frac{E_1\nu}{1-\nu^2} + Z_1E_{1s}\left(\sin^2\theta\cos\theta + \sin^2\beta\cos\beta\right)$$

$$J_{15} = \frac{E_2\nu}{1-\nu^2} + Z_1E_{2s}\left(\sin^2\theta\cos\theta + \sin^2\beta\cos\beta\right)$$

$$J_{21} = \frac{E_1\nu}{1-\nu^2} + Z_2E_{1s}\left(\sin\theta\cos^2\theta + \sin\beta\cos^2\beta\right)$$

$$J_{24} = \frac{E_2\nu}{1-\nu^2} + Z_2E_{2s}\left(\sin\theta\cos^2\theta + \sin\beta\cos^2\beta\right)$$

$$J_{33} = \frac{E_1}{2(1+\nu)} + 2Z_3E_{1s}\left(\sin\theta\cos\theta + \sin\beta\cos\beta\right)$$

$$J_{36} = \frac{E_2}{2(1+\nu)} + 2Z_3E_{2s}\left(\sin\theta\cos\theta + \sin\beta\cos\beta\right)$$

$$J_{42} = \frac{E_3\nu}{1-\nu^2} + Z_1E_{3s}\left(\sin^2\theta\cos\theta + \sin^2\beta\cos\beta\right)$$

$$J_{51} = \frac{E_3\nu}{1-\nu^2} + Z_2E_{3s}\left(\sin\theta\cos^2\theta + \sin\beta\cos^2\beta\right) \quad \text{(B.3)}$$

$$J_{63} = \frac{E_3}{2(1+\nu)} + 2Z_3E_{3s}\left(\sin\theta\cos\theta + \sin\beta\cos\beta\right)$$

$$J_{11} = \frac{E_1}{1-\nu^2} + Z_1E_{1s}\left(\cos^3\theta + \cos^3\beta\right)?$$

$$J_{14} = \frac{E_2}{1-\nu^2} + Z_1E_{2s}\left(\cos^3\theta + \cos^3\beta\right)?$$

$$J_{22} = \frac{E_1}{1-\nu^2} + Z_2E_{1s}\left(\sin^3\theta + \sin^3\beta\right)$$

$$J_{25} = \frac{E_2}{1-\nu^2} + Z_2E_{2s}\left(\sin^3\theta + \sin^3\beta\right)$$

$$J_{41} = \frac{E_3}{1-\nu^2} + Z_1E_{3s}\left(\cos^3\theta + \cos^3\beta\right)$$

$$J_{55} = \frac{E_3}{1-\nu^2} + Z_2E_{3s}\left(\sin^3\theta + \sin^3\beta\right)$$

where

$$Z_1 = \frac{d\sin(q+b)}{s[\sin(q) + \sin(b)]}$$

$$Z_2 = \frac{d\sin(q+b)}{s[\mathrm{os}(q) + \cos(b)]} \quad \text{(B.4)}$$

$$Z_3 = \frac{d\sin(q+b)}{2s}$$

In Eq. (B.3):

$$E_1 = \int_{-h/2}^{h/2} E_{sh}(z)dz = \left(E_c + \frac{E_m - E_c}{K_{sh}+1}\right)h$$

$$E_2 = \int_{-h/2}^{h/2} zE_{sh}(z)dz = \frac{(E_m - E_c)kh^2}{2(K_{sh}+1)(K_{sh}+2)}$$

$$E_3 = \int_{-\frac{h}{2}}^{\frac{h}{2}} z^2E_{sh}(z)dz = \left[\frac{E_c}{12} + (E_m - E_c)\left(\frac{1}{K_{sh}+3} + \frac{1}{K_{sh}+2} + \frac{1}{4K_{sh}+4}\right)\right]h^3 \quad \text{(B.5)}$$

External Stiffeners:

$$E_{1s} = \int_{-\left(\frac{h}{2}+h_s\right)}^{-\frac{h}{2}} E_s\,(z)dz = \left(E_m + \frac{E_c - E_m}{K_{st}+1}\right)h_s$$

$$E_{2s} = \int_{-\left(\frac{h}{2}+h_s\right)}^{-\frac{h}{2}} zE_s\,(z)dz = \frac{E_m}{2}\ \ hh_s\left(\frac{h_s}{h}+1\right)$$

$$+(E_c - E_m)\ \ hh_s\left(\frac{1}{K_{st}+2}\frac{h_s}{h} + \frac{1}{2K_{st}+2}\right)$$

$$E_{3s} = \int_{-\left(\frac{h}{2}+h_s\right)}^{-\frac{h}{2}} z^2E_s\,(z)dz =$$

$$\frac{E_m}{3}h_s^3\left(\frac{3}{4}\frac{h^2}{h_s^2} + \frac{3}{2}\frac{h}{h_s} + 1\right)$$

$$+(E_c - E_m)h_s^3\left[\frac{1}{K_{st}+3} + \frac{1}{K_{st}+2}\frac{h}{h_s}\right.$$

$$\left. + \frac{1}{4(K_{st}+1)}\frac{h^2}{h_s^2}\right]$$

Internal Stiffeners:

$$E_{1s} = \int_{\frac{h}{2}}^{\frac{h}{2}+h_s} E_s\,(z)dz = \left(E_c + \frac{E_m - E_c}{K_{st}+1}\right)h_s$$

$$E_{2s} = \int_{\frac{h}{2}}^{\frac{h}{2}+h_s} zE_s\,(z)dz = \frac{E_c}{2}\ \ hh_s\left(\frac{h_s}{h}+1\right)$$

$$+(E_m - E_c)\ \ hh_s\left(\frac{1}{K_{st}+2}\frac{h_s}{h} + \frac{1}{2K_{st}+2}\right)$$

$$E_{3s} = \int_{\frac{h}{2}}^{\frac{h}{2}+h_s} z^2E_s\,(z)dz =$$

$$\frac{E_c}{3}h_s^3\left(\frac{3}{4}\frac{h^2}{h_s^2} + \frac{3}{2}\frac{h}{h_s} + 1\right)$$

$$+(E_m - E_c)h_s^3\left[\frac{1}{K_{st}+3} + \frac{1}{K_{st}+2}\frac{h}{h_s}\right.$$

$$\left. + \frac{1}{4(K_{st}+1)}\frac{h^2}{h_s^2}\right]$$